Electronic Supplementary Material (ESI) for Physical Chemistry Chemical Physics.

Chemical exchange at the ferroelectric phase transition of lead germanate revealed by solid state ^{207}Pb nuclear magnetic resonance

Supplementary Information

Claudia E. Avalos, Brennan J. Walder, Jasmine Viger-Gravel, Arnaud Magrez and Lyndon Emsley

Institut des Sciences et Ingénierie Chimiques, Ecole Polytechnique Fédérale de Lausanne (EPFL), CH-1015 Lausanne, Switzerland

I. X-RAY CRYSTALLOGRAPHY

We measured our lead germanate samples using X-ray powder diffraction, the results are shown below:

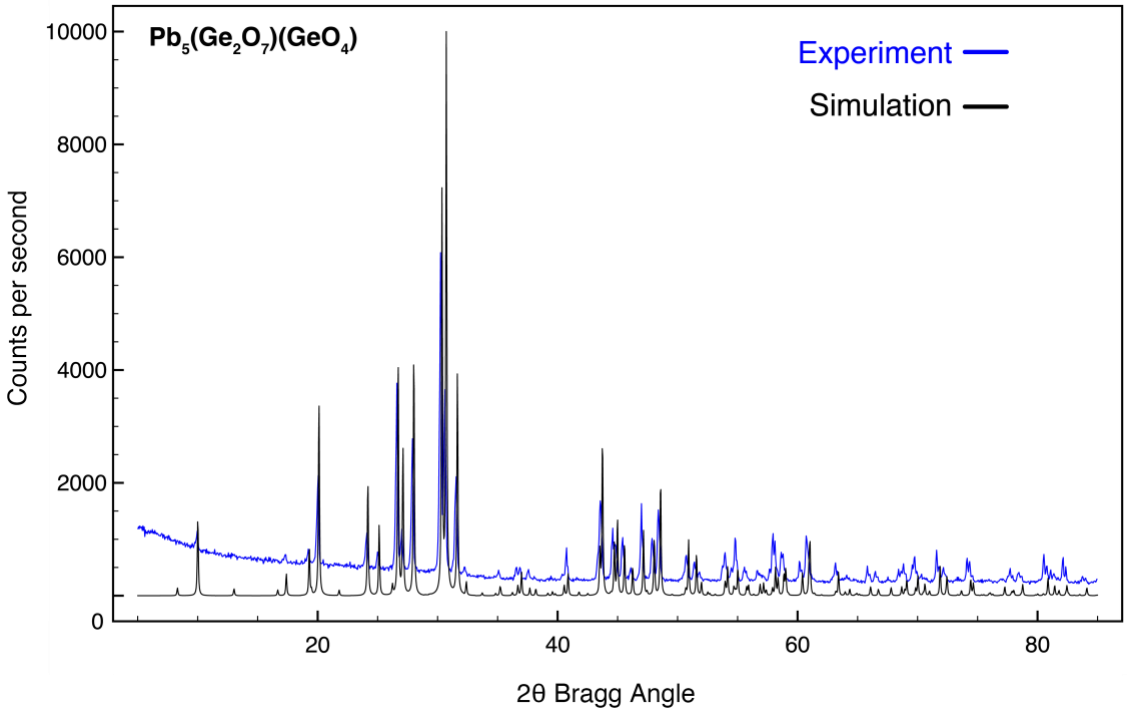

FIG. S1. X-ray powder diffraction of lead germanate. Experimental pXRD (blue trace) of a lead germanate powder is compared with simulations. Experiments were carried out using a X'Pert MPD PRO (Panalytical) diffractometer equipped with a ceramic tube (Cu anode, λ = 1.54060 Å), a secondary graphite (002) monochromator and an RTMS X'Celerator (Panalytical) in an angle range of $2\theta = 5^{\circ}$ to 90°, by step scanning with a step of 0.01 degree. Simulations (black trace) were generated using Mercury software available from Cambridge Crystallographic Data Centre based on atomic coordinates obtained from single crystal X-ray from Kay et al.[1]

II. DENSITY FUNCTIONAL THEORY CALCULATIONS

^{207}Pb magnetic shielding tensors were calculated using the Amsterdam Density Functional (ADF) package[2-4]. These calculations included relativistic spin-orbit corrections via the zeroth-order regular approximation (ZORA)[5-8] since the contribution of shielding due to a relativistic nature is important for heavy nuclei and Grimme's[9] dispersion correction. The revised BP86 generalized gradient approximation (GGA) exchange-correlation functional was used with the ZORA triple zeta basis set for the magnetic shielding calculation.

Large cluster models that include relativistic spin-orbit coupling corrections have been shown to lead to calculated shielding values that correlate best to experimental chemical shifts for heavy nuclei, hence we took this approach to calculate chemical shift values for the ^{207}Pb nuclei in lead germanate. Cluster models were built for each crystallographically distinct Pb(II) site from atomic coordinates determined from neutron diffraction measurements of the ferroelectric form of $Pb_5(Ge_2O_7)(GeO_4)$.[1]

Alkan and Dybowski[10-11] demonstrated that cluster size has an important effect on the calculated NMR parameters (due to long range effects of the heavy atom lead) and that a minimum of three coordination shells is required in the cluster model in order to reproduce experimental results. To achieve self-consistent field (SCF) convergence in clusters of ionic solid networks, it is important to minimize the charge, and to define the electron density distribution to properly fill the HOMO/LUMO orbitals. Usually, the clusters can be capped with hydrogens to balance the charges and remove the dangling bonds. Here, the addition of hydrogen to the lead clusters did not balance the charges. Methods developed by Alkan and Dybowski counter this effect by either increasing the charge at the terminating nuclei by +1 or by modifying the terminal atom by the sum of the bond strength of the atom. However, these methods were not implemented.

Here two sets of cluster models were generated. In one case we explored a cluster model for which the cluster contained only the first coordination shell around the lead atom, truncating any magnetic couplings from other atoms at distances greater than ~ 4 Å from the lead nucleus. The second set of cluster models were generated which incorporated two-coordination shells around the central atom of Pb(II).

A simple formula relates the shielding components to the chemical shift components:

$$\delta_{iso} = \frac{\sigma_{ref} - \sigma_{iso}}{1 - \sigma_{ref}}. \qquad \textbf{(EQ. S1)}$$

Where δ_{iso} is the isotropic chemical shift and σ_{iso} is the isotropic shielding component. No suitable reference exists for lead, hence the calculated isotropic shielding value is calculated for $Pb(CH_3)_4$ using the same level of theory and basis set as for the lead germanate calculations (where δ_{iso} = 0 ppm for $Pb(CH_3)_4$ (σ_{ref}). Our calculations using a three shell model did not converge and calculations done with a one and two shell coordination model did not correlate well with observed isotropic shielding and isotropic shifts. We note, that the unit cell of lead germanate contains nine crystallographically distinct lead nuclei, and this led to numerous difficulties related to charge assignments and computational time required to explore each cluster model. No reliable Pb-207 NMR parameters were obtained (Fig. S2). ^{207}Pb site assignments of the spectra were instead made on the basis of changes in the NMR spectra in the paraelectric and ferroelectric phases and comparison to literature X-ray data.

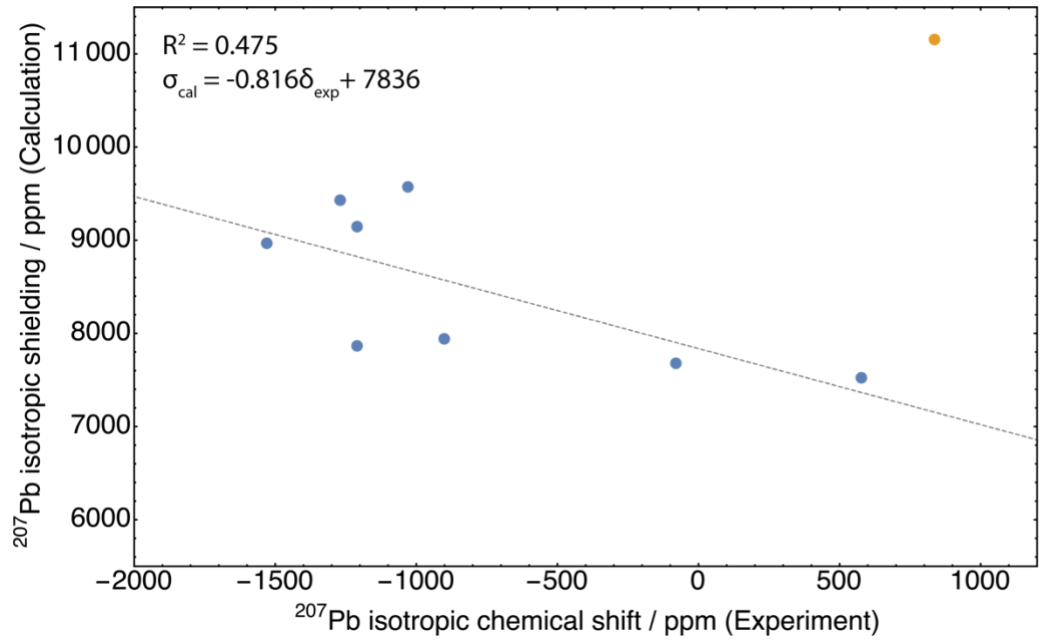

FIG. S2. Calculated ^{207}Pb chemical shielding values and measured chemical shift values using a cluster model with 1 coordination shell. The equation of the correlation line for the model is shown on the plot as well as the R^2 value.

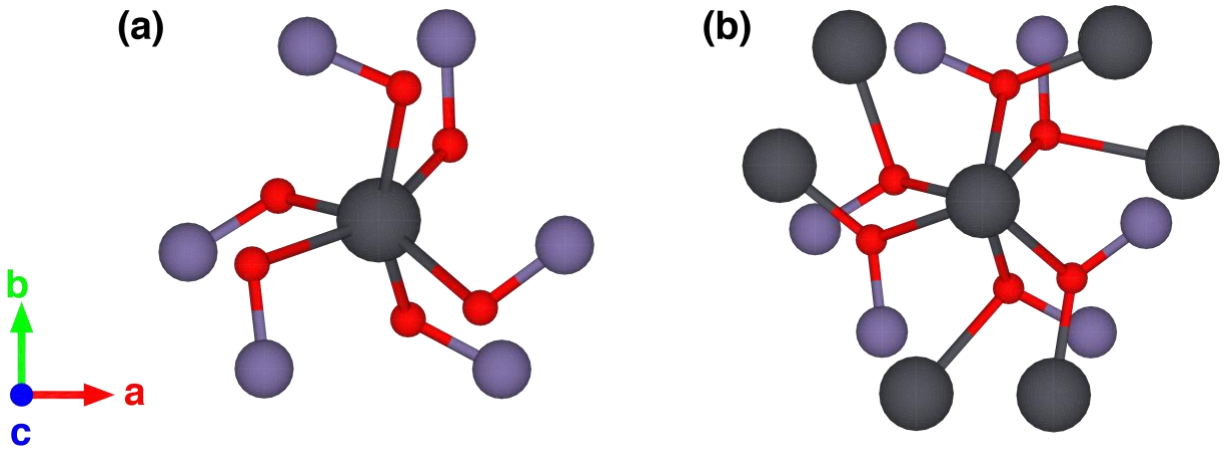

FIG. S3. For Pb site 2B: (a) 1 coordination shell cluster. (b) 2 coordination shell cluster.

III. ELECTRON PARAMAGNETIC RESONANCE MEASUREMENTS

We performed electron paramagnetic resonance measurements on single crystals of our lead germanate samples and found strong EPR signals, likely due to paramagnetic defects. Such defects may be responsible for relatively short ^{207}Pb transverse coherence lifetimes estimated to be on the order of one millisecond. Experiments were done on a single crystal of lead germanate with the c-axis oriented along the magnetic field direction. We used a Bruker Elexys X-Band spectrometer console and performed the measurement at 20 K.

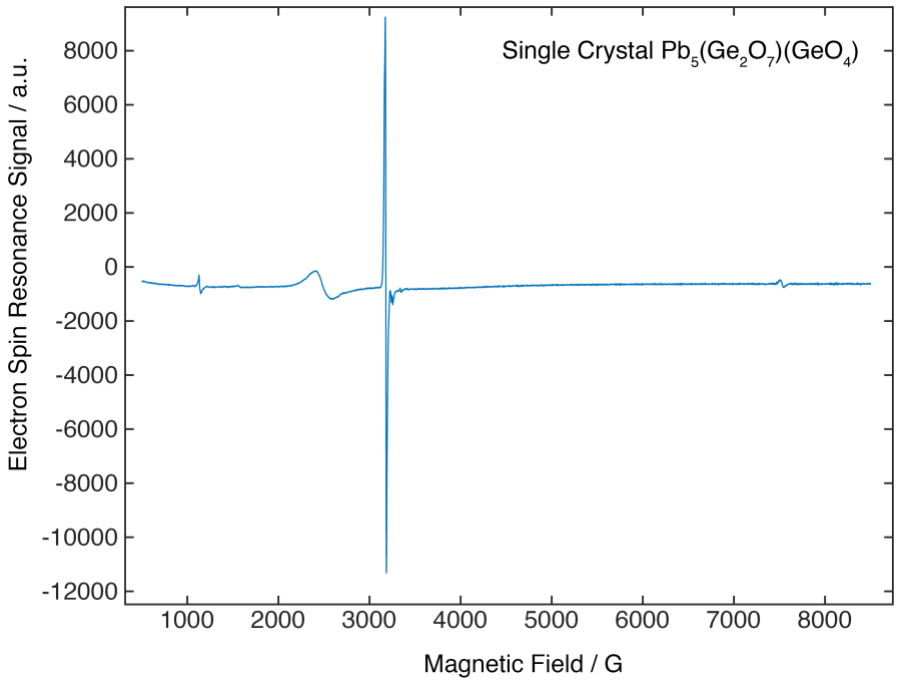

FIG. S4. Presence of paramagnetic defects in lead germanate crystal. The sharp signal near 3 kG is orientation dependent, the intensity of this signal is maximized when the c-axis of the crystal is along the magnetic field, indicating the presence of a paramagnetic defect oriented along one of the crystallographic axes. Peaks at 1 kG and 7.5 kG indicate the presence of hyperfine coupling, likely to a ^{207}Pb spin 1/2 nucleus. The broad beak at 2.5 kG was not orientation dependent and was not present in a background spectrum, indicative that it is a non-oriented defect in the crystal lattice. Spectrum taken at 20 K at X-Band on Bruker Elexys 580 spectrometer.

IV. NUCLEAR MAGNETIC RESONANCE MEASUREMENTS

We have included here the TOP-aMAT spectra collected at each temperature, along with the corresponding sideband dimension fits done for each lead site.

High spinning speeds can cause chemical shift changes in lead containing ferroelectric materials . We observe additional resonances near -1300 ppm when we compare isotropic spectra at 20 kHz versus 12.5 kHz, as shown in Fig. S5. Note that in this region, we predict that site 2A, 2B, and 3A will be nearly overlapping. One possible explanation, is that sites 2A and 2B possess short transverse relaxation times (T_2) and are observed more strongly when the TOP-aMAT mixing period is shorter (mixing periods are 560 µs and 350 µs for 12.5 kHz and 20 kHz MAS, respectively). This explanation is consistent with our stipulation that sites 2A and 2B are difficult to resolve in our spectra.

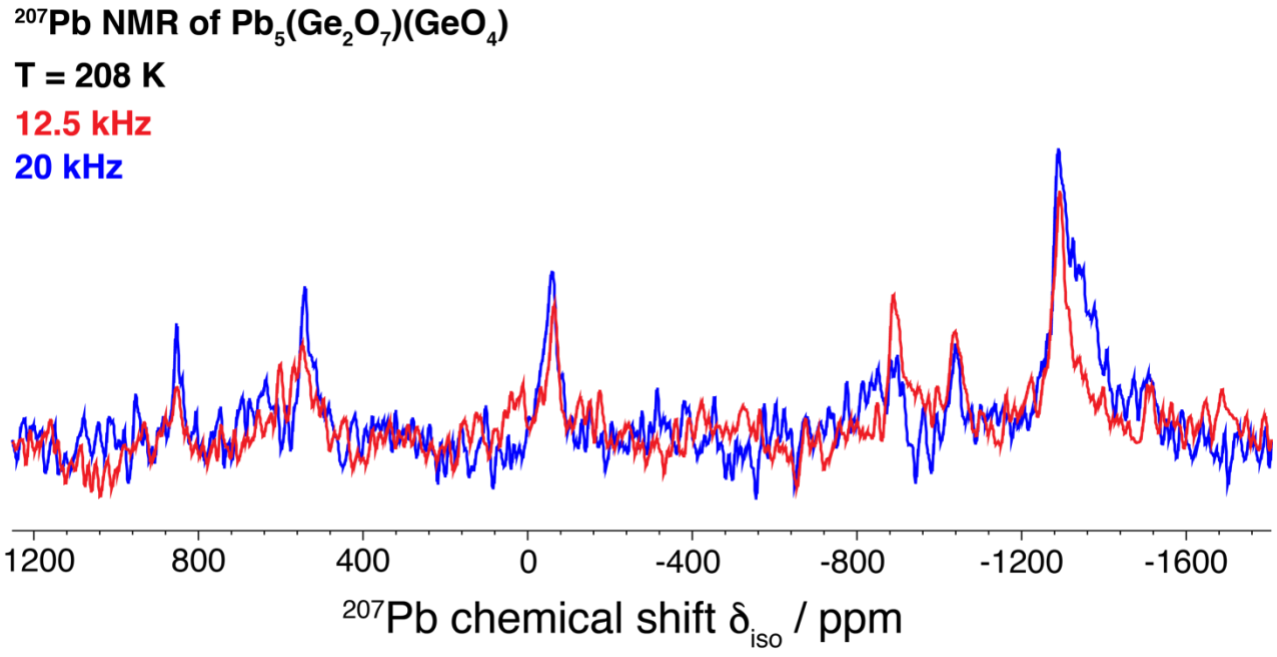

FIG. S5. Projection of chemical shift components from TOP-aMAT 208 K spectrum (figure S6). Comparison of ^{207}Pb chemical shifts at two spinning speeds, 12.5 kHz and 20 kHz at 208 K. We observe additional sites near -1300 ppm as we increase the MAS speed to 20 kHz.

The evolution of the shielding anisotropy and chemical shift for each lead site as a function of temperature can be seen in Figure S6 below, which shows the TOP-aMAT spectra taken at each temperature. Fits to the sideband profiles of each lead site are shown in Figure S7. Parameter tables for these measurements are shown in Table S5.

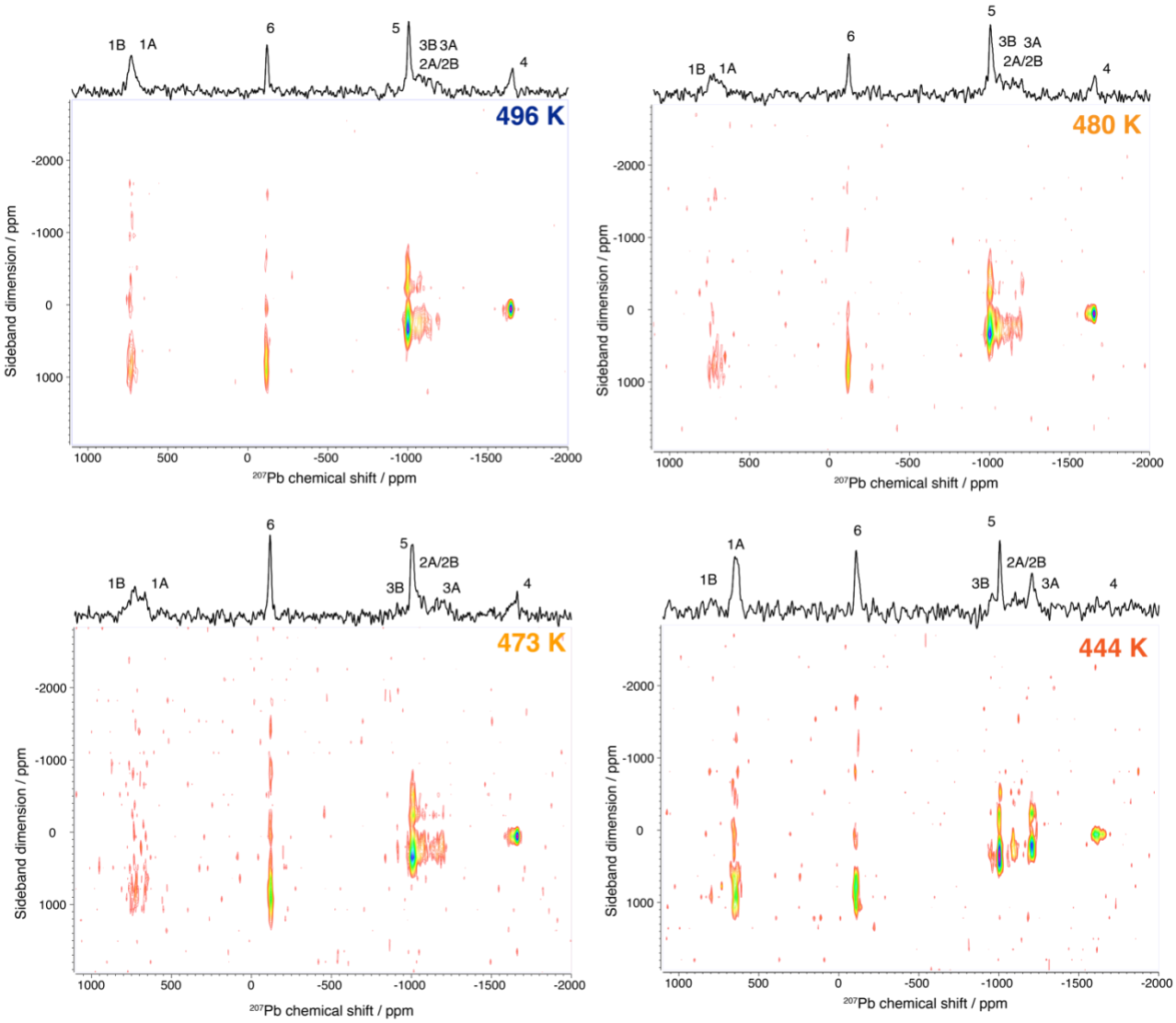

FIG. S6. ^{207}Pb NMR TOP-aMAT spectra of lead germanate. The temperature of each measurement is indicated in the upper right hand corner of each spectrum. Peaks in the isotropic spectra are labeled with our proposed assignments. All of the experiments shown here were done with 12.5 kHz MAS frequency.

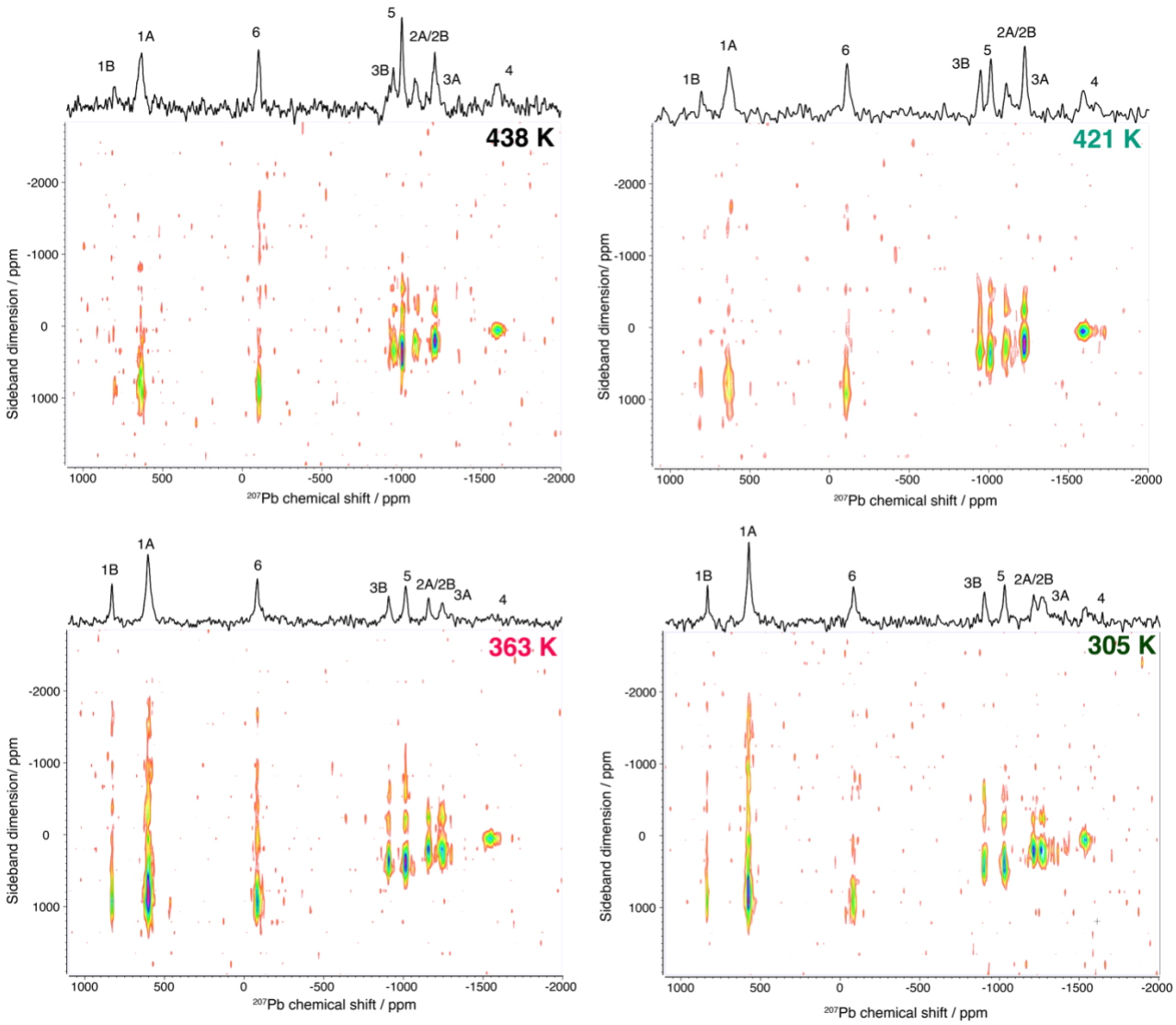

FIG. S6 (continued). ^{207}Pb NMR TOP-aMAT spectra of lead germanate. Temperatures are indicated on the right hand corner of each spectrum. Proposed site assignments are labeled for each spectrum. All of the experiments shown here were done with 12.5 kHz MAS frequency.

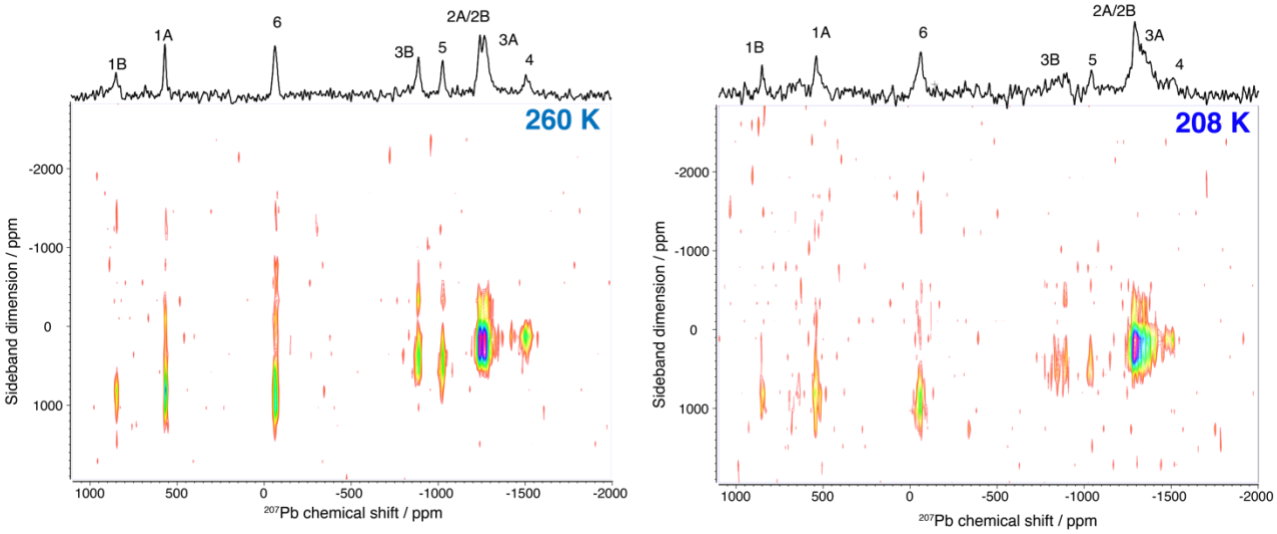

FIG. S6 (continued). ^{207}Pb NMR TOP-aMAT spectra of lead germanate. Measurements taken at 260 K,208 K as indicated on the right hand corner of each spectrum. Proposed site assignments are labeled for each spectrum. Experiments at 208 K and 260 K were done at MAS of 20 kHz.

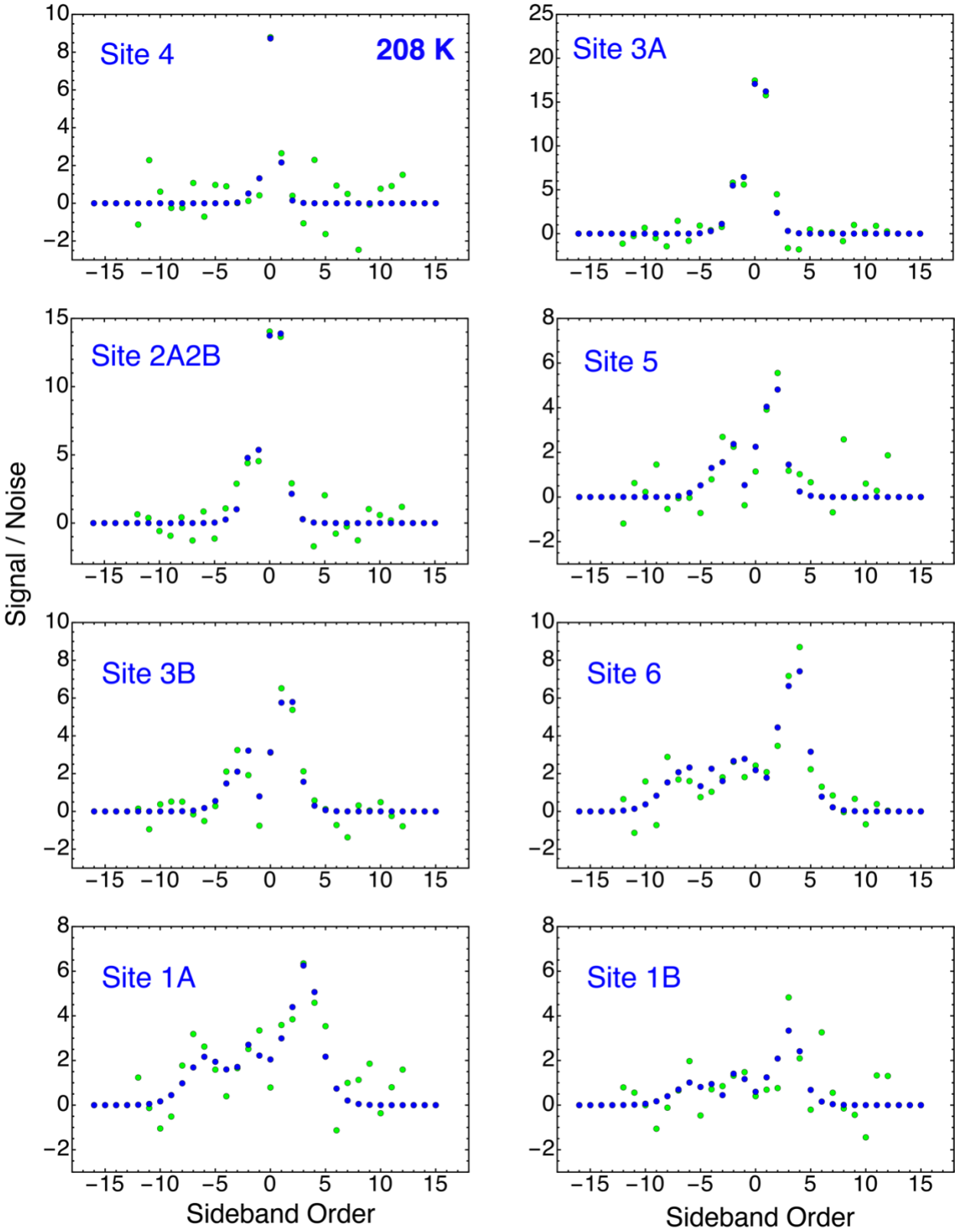

FIG. S7. Results from sideband fits of TOP-aMAT sideband dimension projection of lead germanate. The blue points indicate the sideband fit, the green points indicate the TOP-aMAT measured sideband projection. The data shown has been normalized with respect to the noise floor, each point indicates a sideband amplitude (shown in terms of signal/noise, y-axis) with the respective sideband order (x-axis). Temperature 208 K (blue labels), 260 K (purple labels), 305 K (light blue label), 363 K (sea green label). Details of the fitting method are described in the methods section of the main text (Section 2.3).

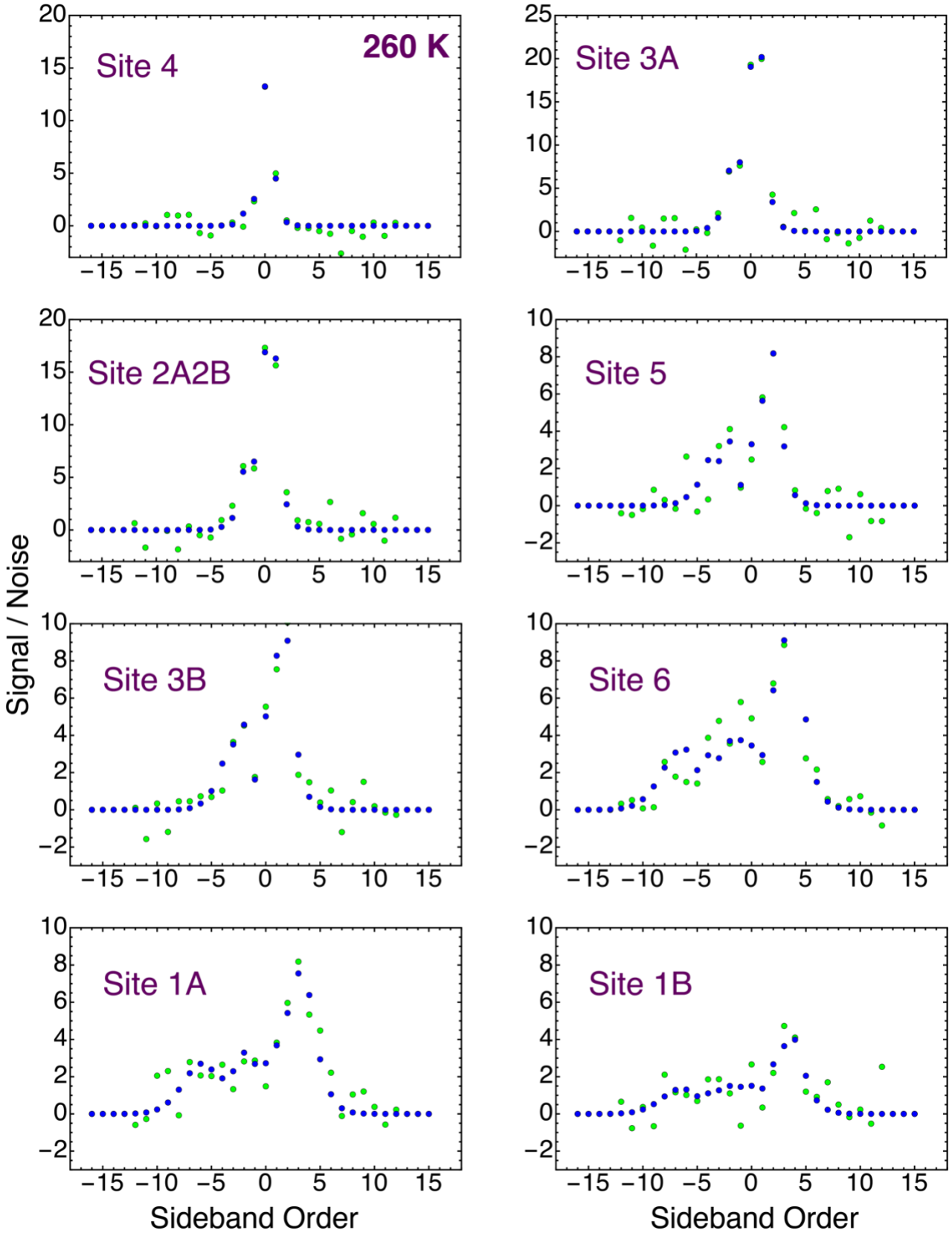

FIG. S7 continued. Sideband fits of TOP-aMAT sideband dimension projection of lead germanate at 260 K.

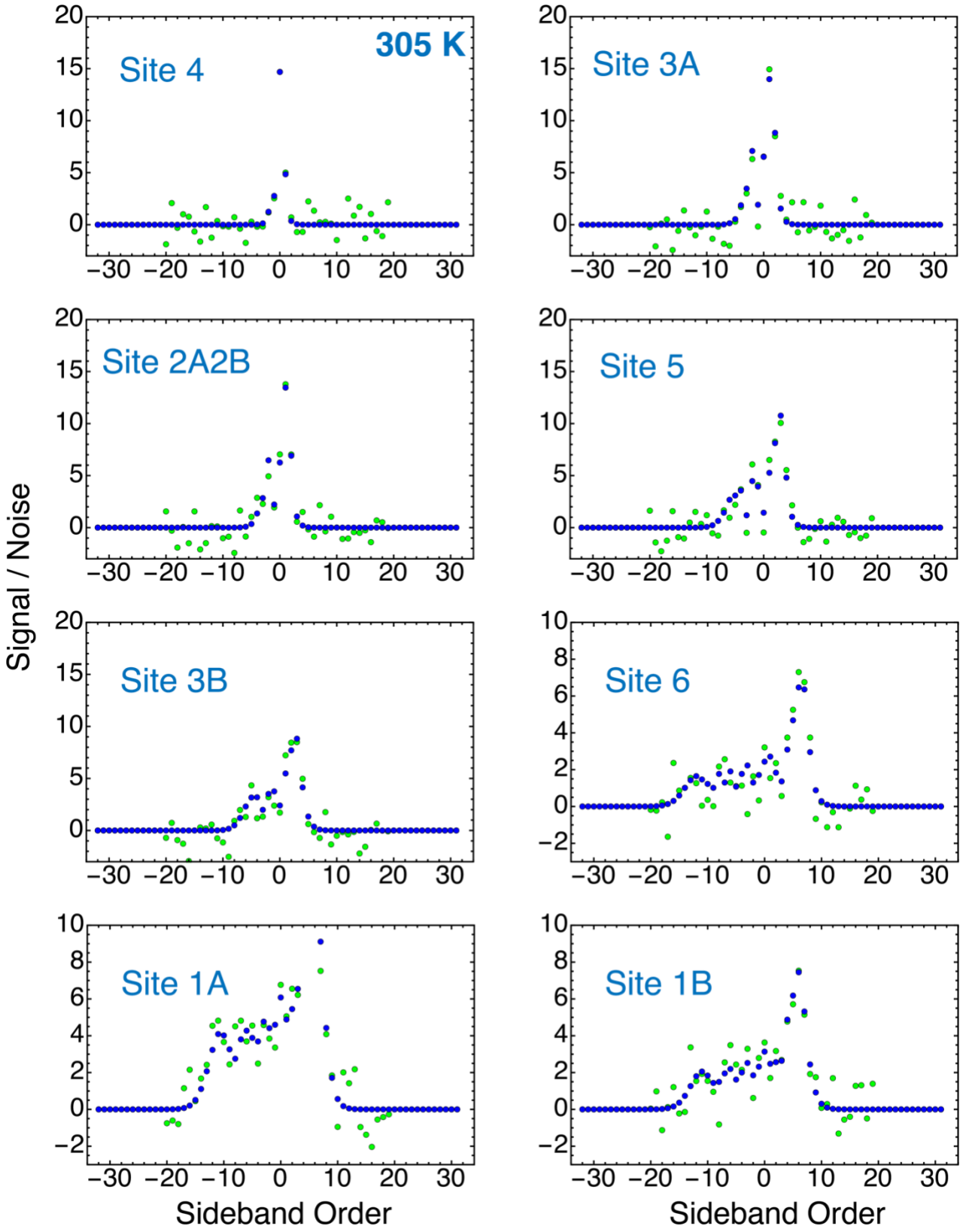

FIG. S7 continued. Sideband fits of TOP-aMAT sideband dimension projection of lead germanate at 305 K.

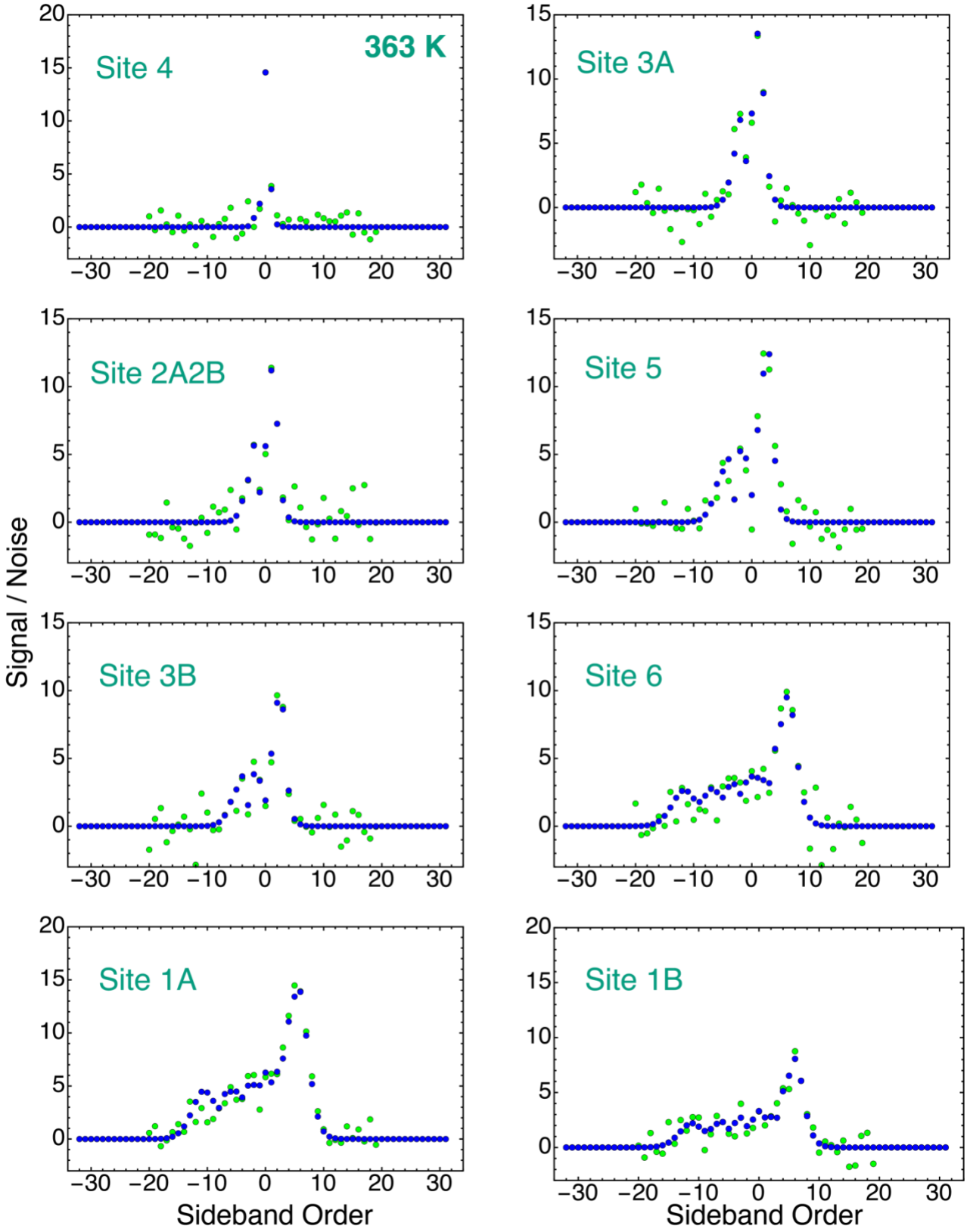

FIG. S7 continued. Sideband fits of TOP-aMAT sideband dimension projection of lead germanate at 363 K.

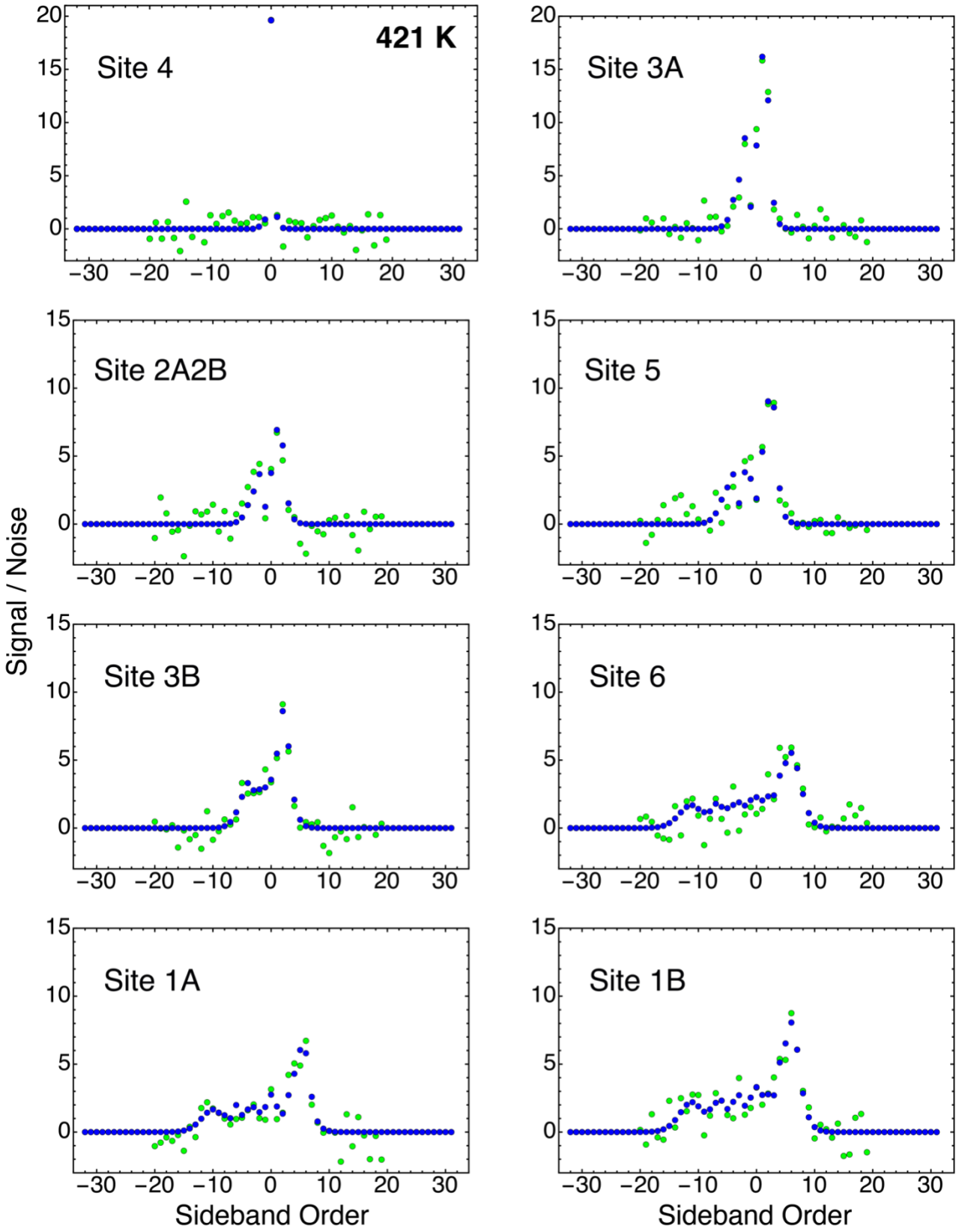

FIG. S7 continued. Sideband fits of TOP-aMAT sideband dimension projection of lead germanate at 421 K.

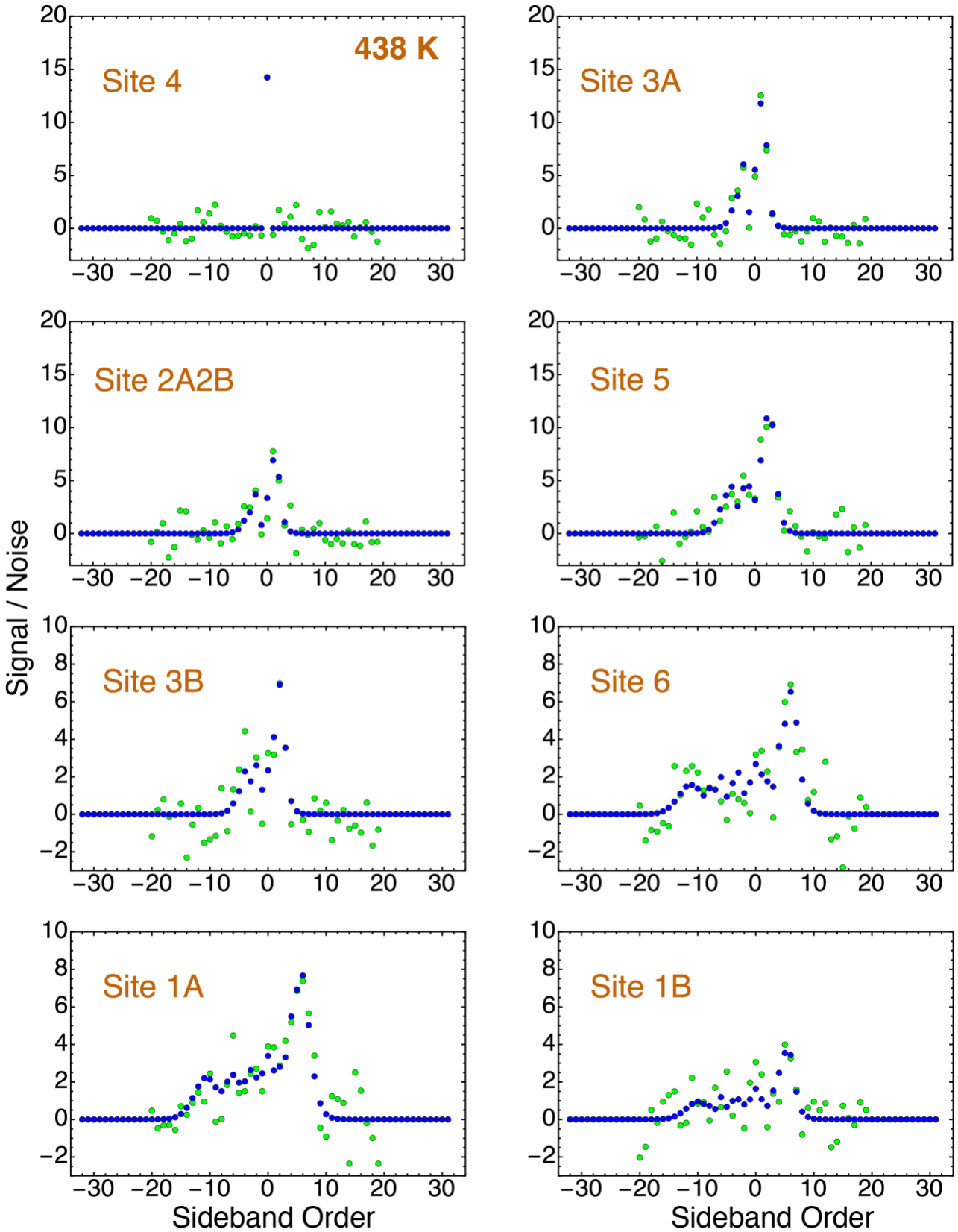

FIG. S7 continued. Sideband fits of TOP-aMAT sideband dimension projection of lead germanate at 438 K.

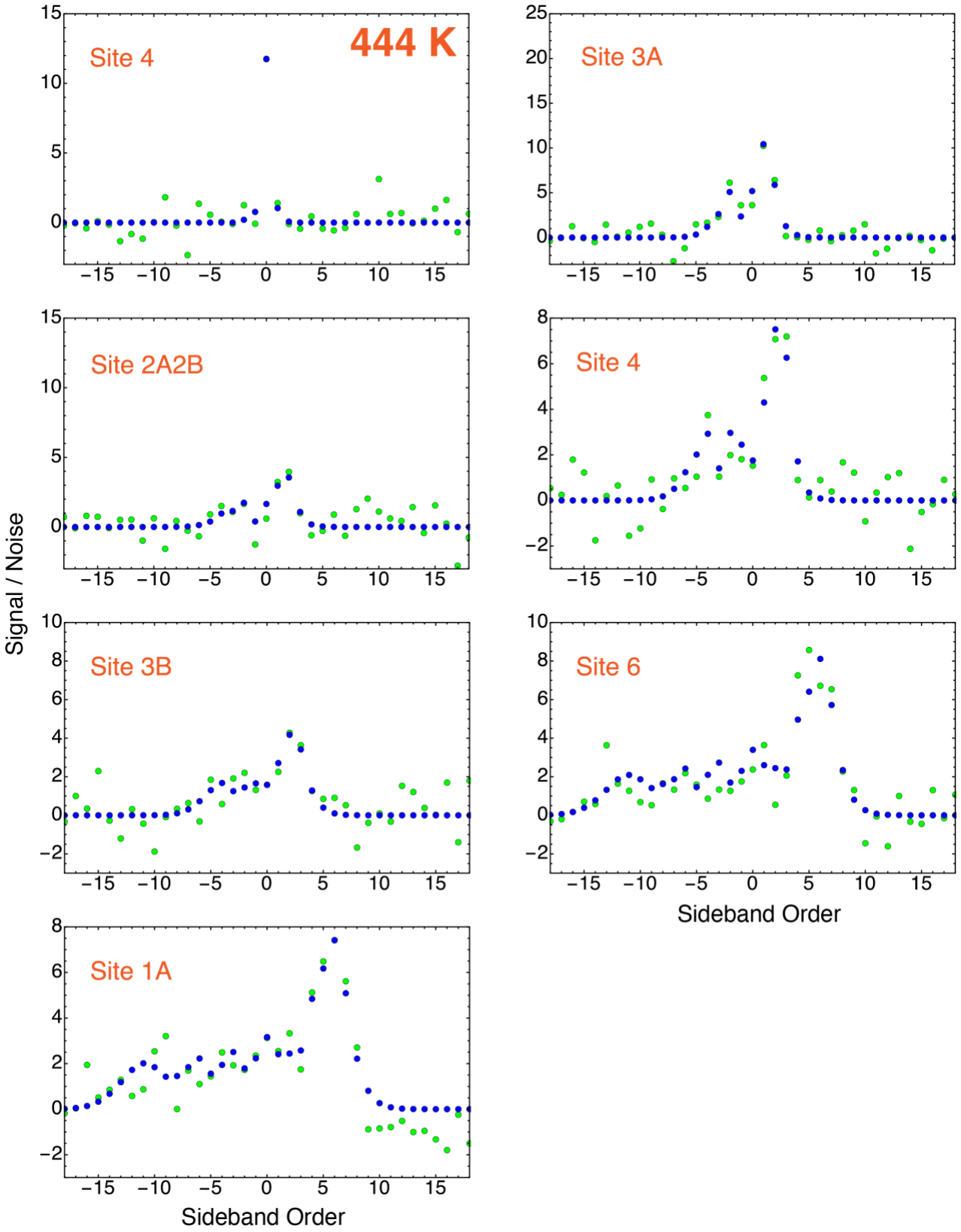

FIG. S7 continued. Sideband fits of TOP-aMAT sideband dimension projection of lead germanate at 444 K.

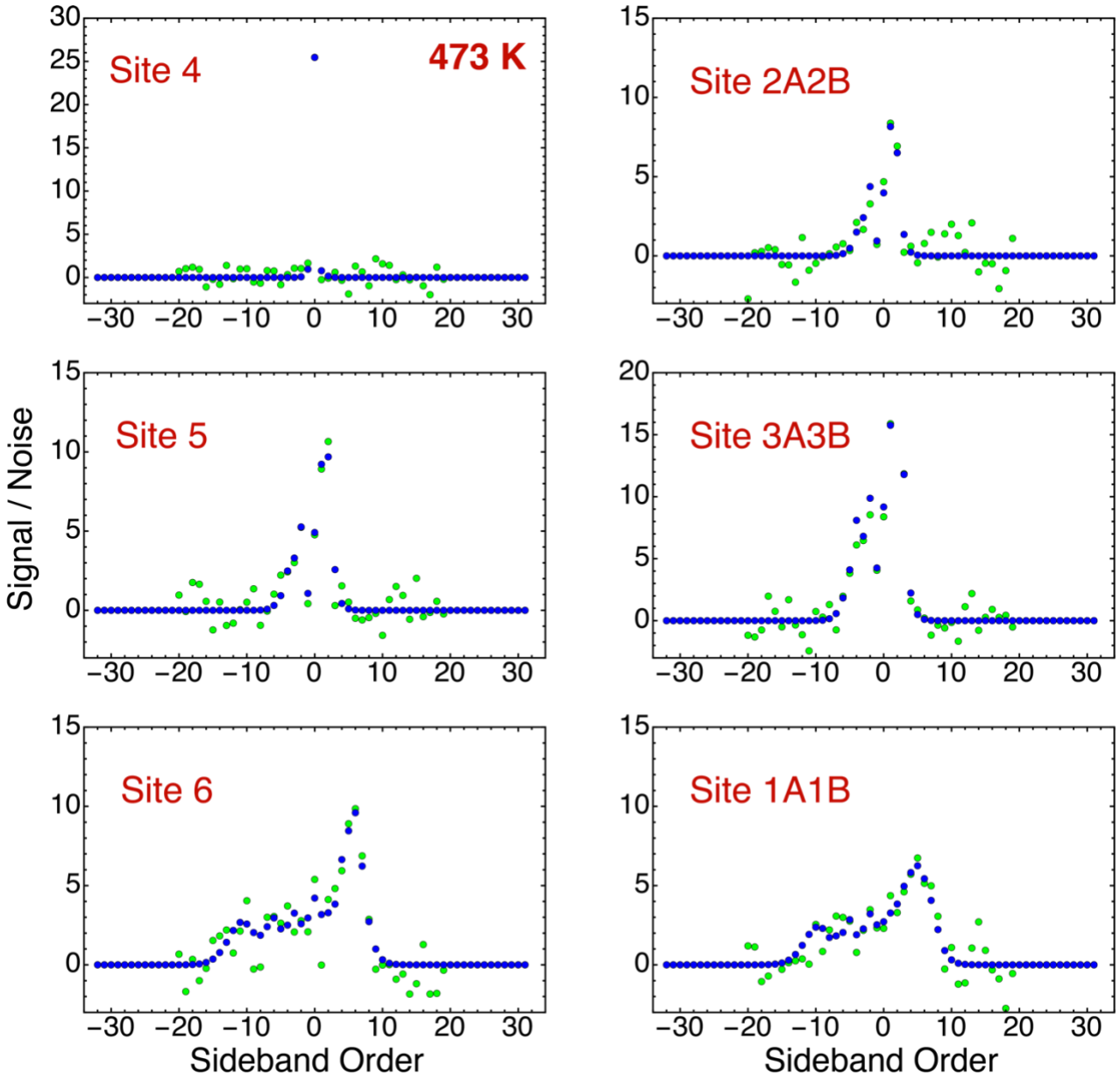

FIG. S7 continued. Sideband fits of TOP-aMAT sideband dimension projection of lead germanate at 473 K.

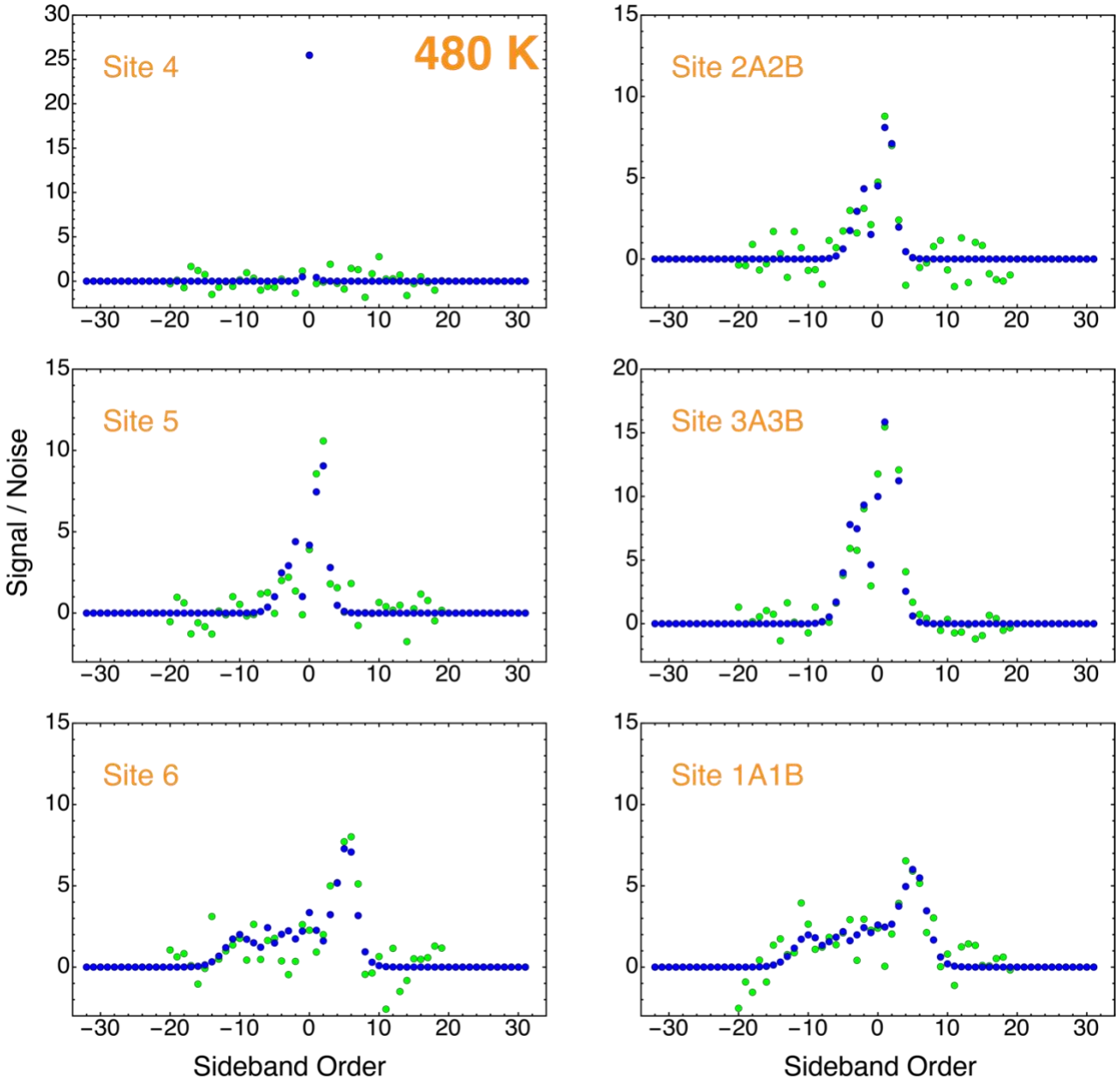

FIG. S7 continued. Sideband fits of TOP-aMAT sideband dimension projection of lead germanate at 480 K.

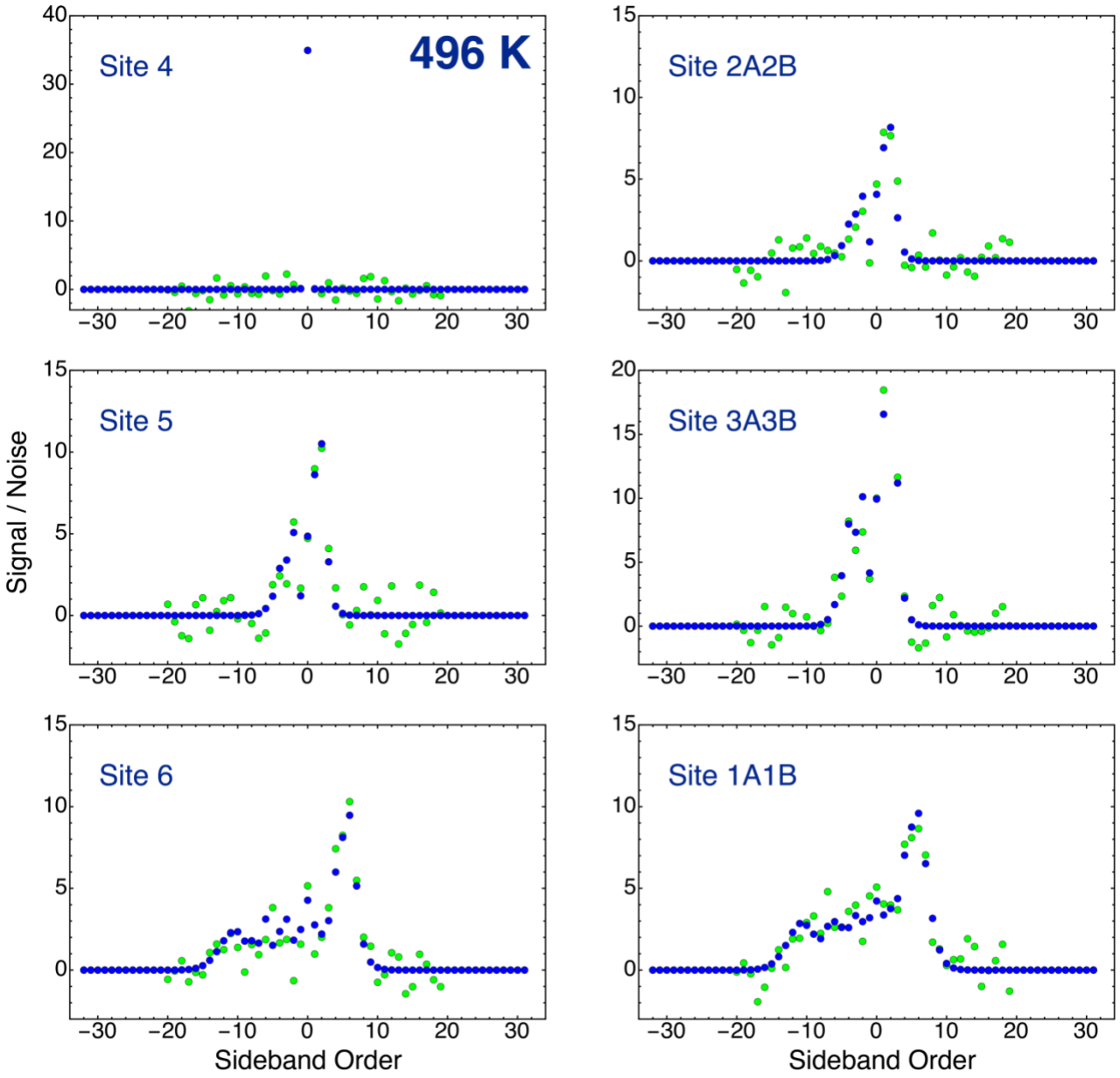

FIG. S7 continued. Sideband fits of TOP-aMAT sideband dimension projection of lead germanate at 496 K.

Table S1: ^{207}Pb δ_{iso} parameters for each lead site in lead germanate at ten different temperatures, referenced to tetramethylead. 1D spectra were projected from 2D TOP-aMAT spectra, apodized with a Gaussian filter and each peak was fit to a Gaussian function or multiple Gaussian functions in the case of overlap. Standard fit errors ranged from 0.1 to 8 ppm, and can be seen on the chemical shift plots for each lead site as well as a subscript in the table below. The isotropic shift of site 1B could not be measured at 444 K.

	^{207}Pb δ_{iso} (ppm)									
Site	208 K	260 K	305 K	363 K	421 K	438 K	444 K	473 K	480 K	496 K
1B	$851.9_{\pm0.7}$	$846.3_{\pm0.5}$	$836.9_{\pm0.5}$	$827.7_{\pm0.4}$	$805.7_{\pm0.6}$	$800.0_{\pm0.7}$	NA	$715.0_{\pm1.5}$	$715.3_{\pm3.3}$	$732.3_{\pm2.0}$
1A	$538.9_{\pm0.8}$	$562.3_{\pm0.1}$	$577.3_{\pm0.3}$	$596.5_{\pm0.4}$	$633.8_{\pm0.4}$	$636.3_{\pm0.5}$	$643.6_{\pm0.5}$	$715.0_{\pm1.5}$	$715.3_{\pm3.3}$	$732.3_{\pm2.0}$
6	$-54.9_{\pm0.6}$	$-71.2_{\pm0.1}$	$-80.0_{\pm0.7}$	$-88.2_{\pm0.8}$	$-107.5_{\pm0.4}$	$-104.3_{\pm0.4}$	$-111.9_{\pm0.4}$	$-120.3_{\pm0.2}$	$-119.2_{\pm0.7}$	$-119.5_{\pm0.6}$
3B	$-845.9_{\pm2.1}$	$-893.2_{\pm0.2}$	$-901.3_{\pm0.4}$	$-913.4_{\pm0.4}$	$-941.2_{\pm0.3}$	$-946.7_{\pm1.2}$	$-1090_{\pm0.5}$	$-1010.0_{\pm0.5}$	$-1008.6_{\pm0.7}$	$-1003.4_{\pm1.0}$
5	$-1040.0_{\pm1.8}$	$-1030.0_{\pm0.1}$	$-1030.0_{\pm0.3}$	$-1020.0_{\pm0.3}$	$-1010.0_{\pm0.3}$	$-1010.0_{\pm0.3}$	$-961.3_{\pm2.0}$	$-1010.0_{\pm0.5}$	$-1008.6_{\pm0.7}$	$-1003.4_{\pm1.0}$
2A/2B	$-1290.0_{\pm0.8}$	$-1240.0_{\pm0.2}$	$-1210.0_{\pm0.7}$	$-1170.0_{\pm0.4}$	$-1110.0_{\pm0.9}$	$-1090.0_{\pm0.4}$	$-1010.0_{\pm0.5}$	$-1010.0_{\pm0.5}$	$-1008.6_{\pm0.7}$	$-1003.4_{\pm1.0}$
3A	$-1340.0_{\pm2.7}$	$-1270.0_{\pm0.3}$	$-1270.0_{\pm1.0}$	$-1250.0_{\pm0.5}$	$-1220.0_{\pm0.3}$	$-1210.0_{\pm0.7}$	$-1210.0_{\pm0.8}$	$-1180.0_{\pm1.5}$	$-1079.5_{\pm8.6}$	$-1089.5_{\pm8.5}$
4	$-1500.0_{\pm1.8}$	$-1520.0_{\pm0.3}$	$-1530.0_{\pm1.5}$	$-1560.0_{\pm1.6}$	$-1590.0_{\pm1.2}$	$-1600.0_{\pm1.1}$	$-1620.0_{\pm1.6}$	$-1660.0_{\pm0.5}$	$-1659.5_{\pm2.0}$	$-1649.5_{\pm1.8}$

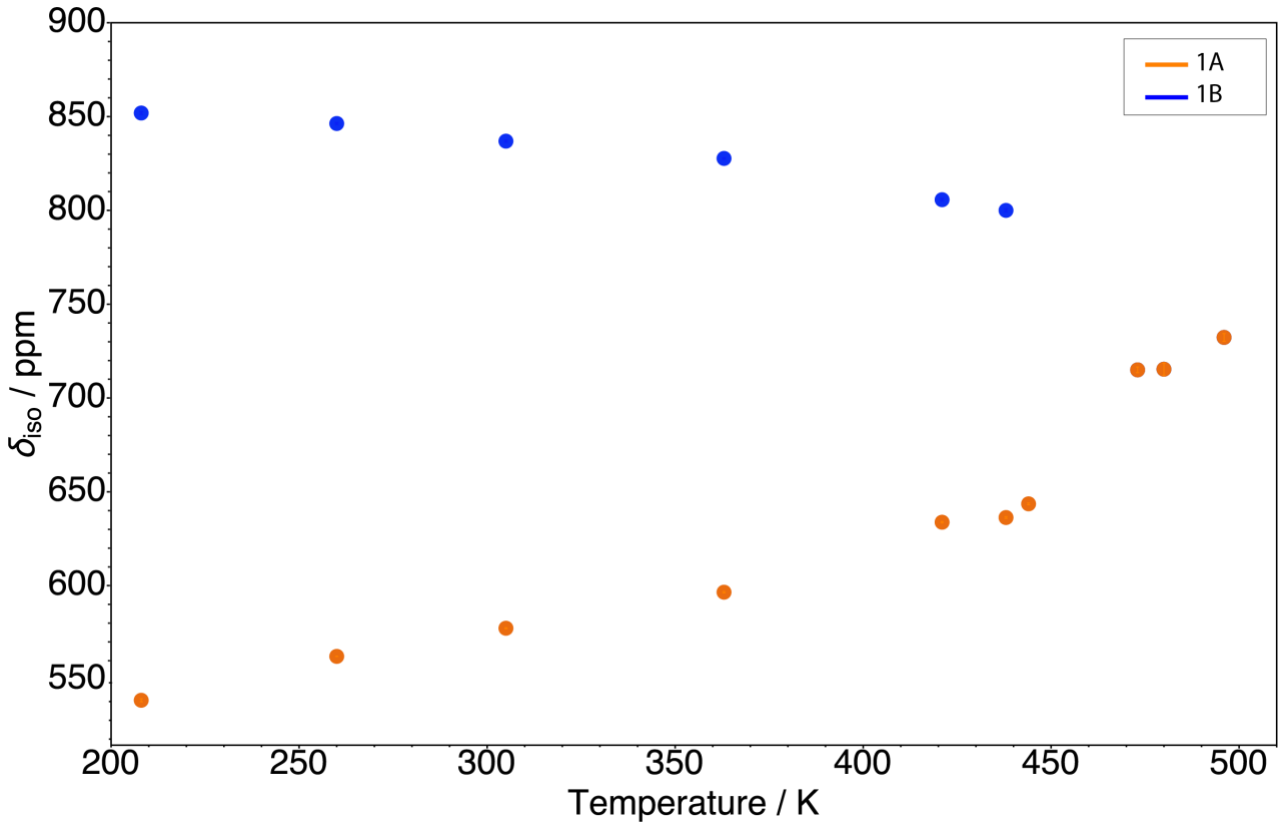

FIG. S8. Temperature induced changes of ^{207}Pb chemical shift parameter δ_{iso} of downfield (deshielded) lead sites in lead germanate. The errors in the fit are shown, these errors are valid for the case of a pure Gaussian lineshape. Sites 1A and 1B coalesce at 473 K. $\Delta\delta_{iso}/\Delta T$ slopes are reported for the range of temperatures between 208 K and 438 K in Table S4.

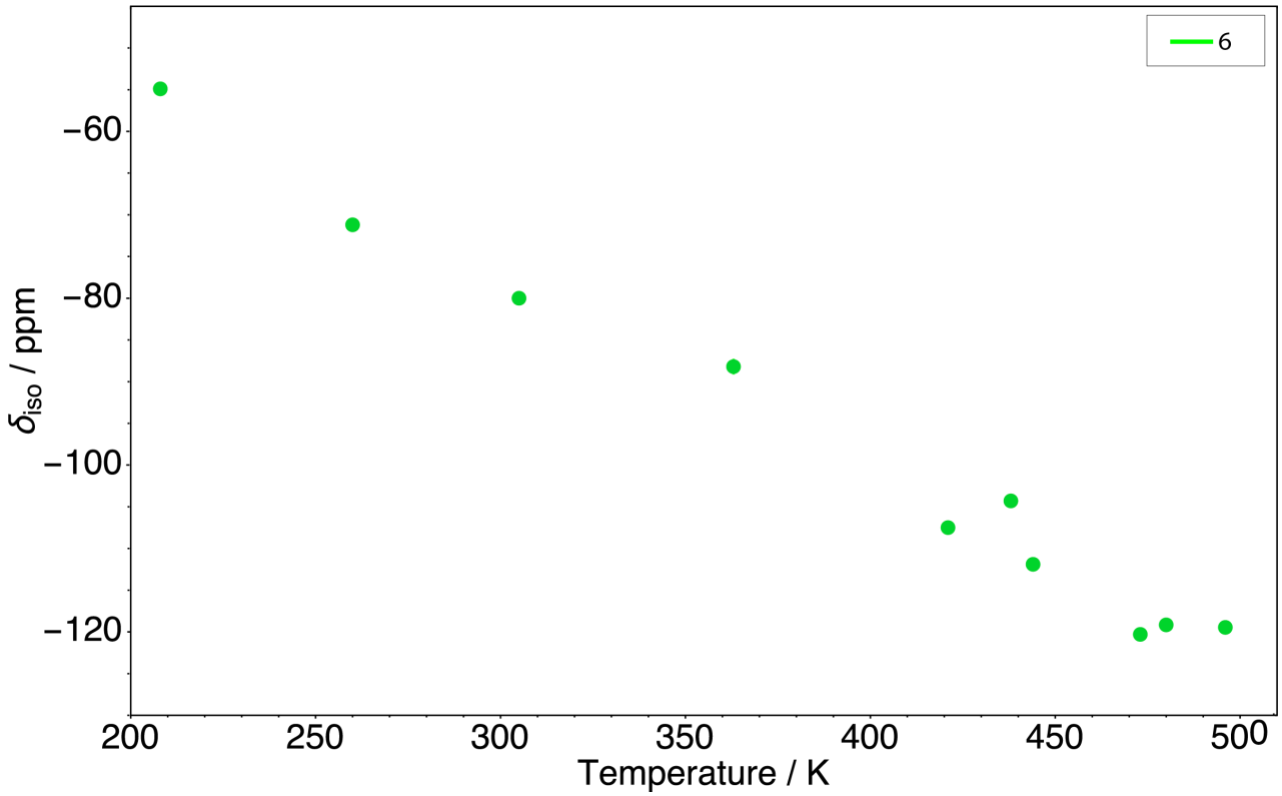

FIG. S8 continued Temperature induced changes of ^{207}Pb chemical shift parameter δ_{iso} of site 6 in lead germanate. The errors in the fit are shown, these errors are valid for the case of a pure Gaussian lineshape.

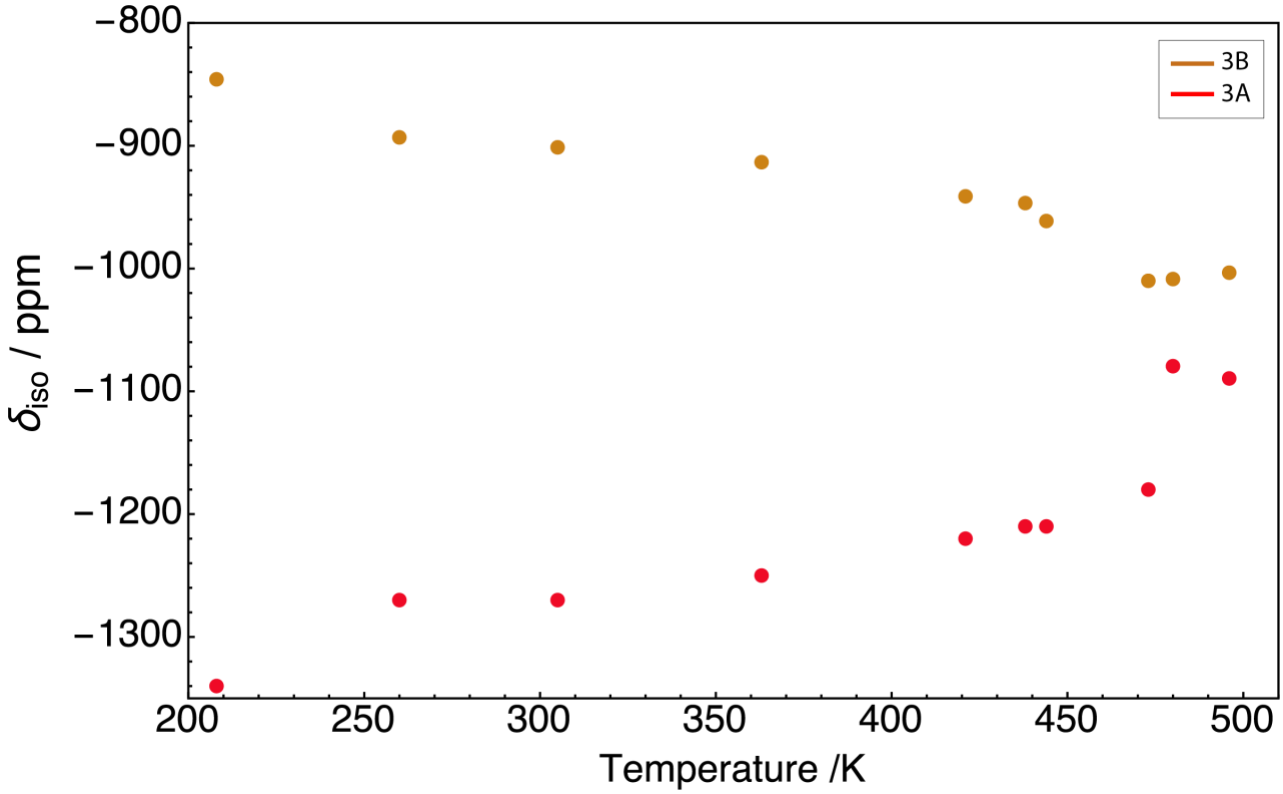

FIG. S8 continued. Temperature induced changes of ^{207}Pb chemical shift parameter δ_{iso} of upfield (shielded) lead sites in lead germanate. Sites 3A and 3B approach coalescence at 473 K, changes in 207Pb chemical shift of these sites remain fairly linear until the phase transition. $\Delta\delta_{iso}/\Delta T$ slopes are reported in Table S4.

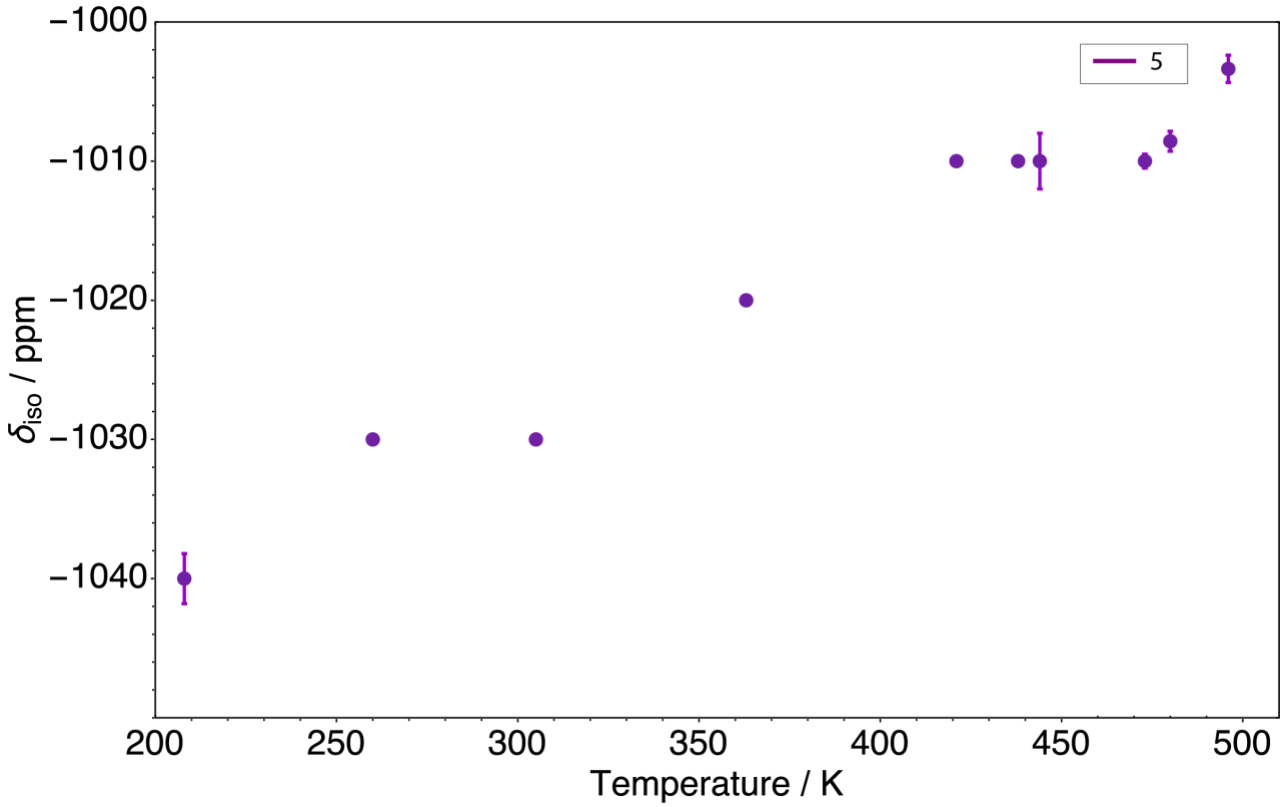

FIG. S8 continued. Temperature induced changes of ^{207}Pb chemical shift parameter δ_{iso} of site 5 in lead germanate.

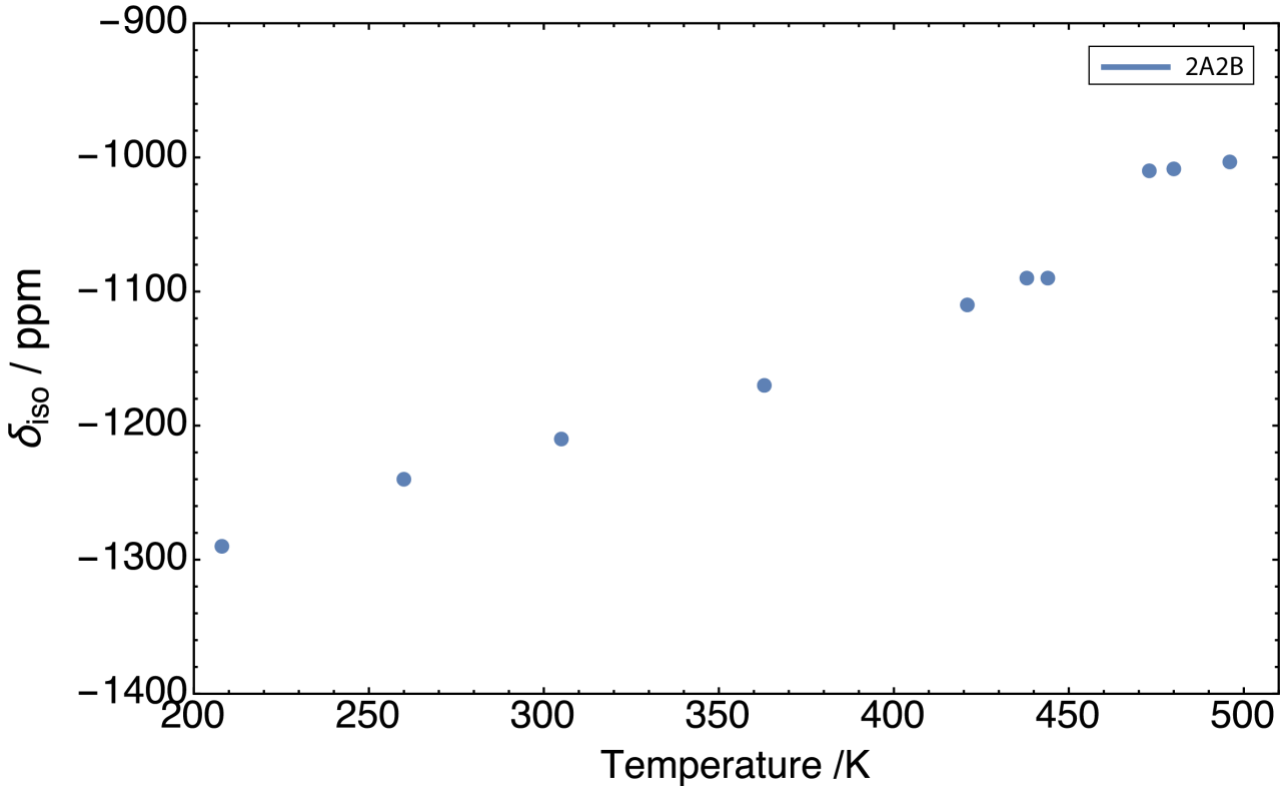

FIG. S8 continued. Temperature induced changes of ^{207}Pb chemical shift parameter δ_{iso} of site 2A or 2B in lead germanate.

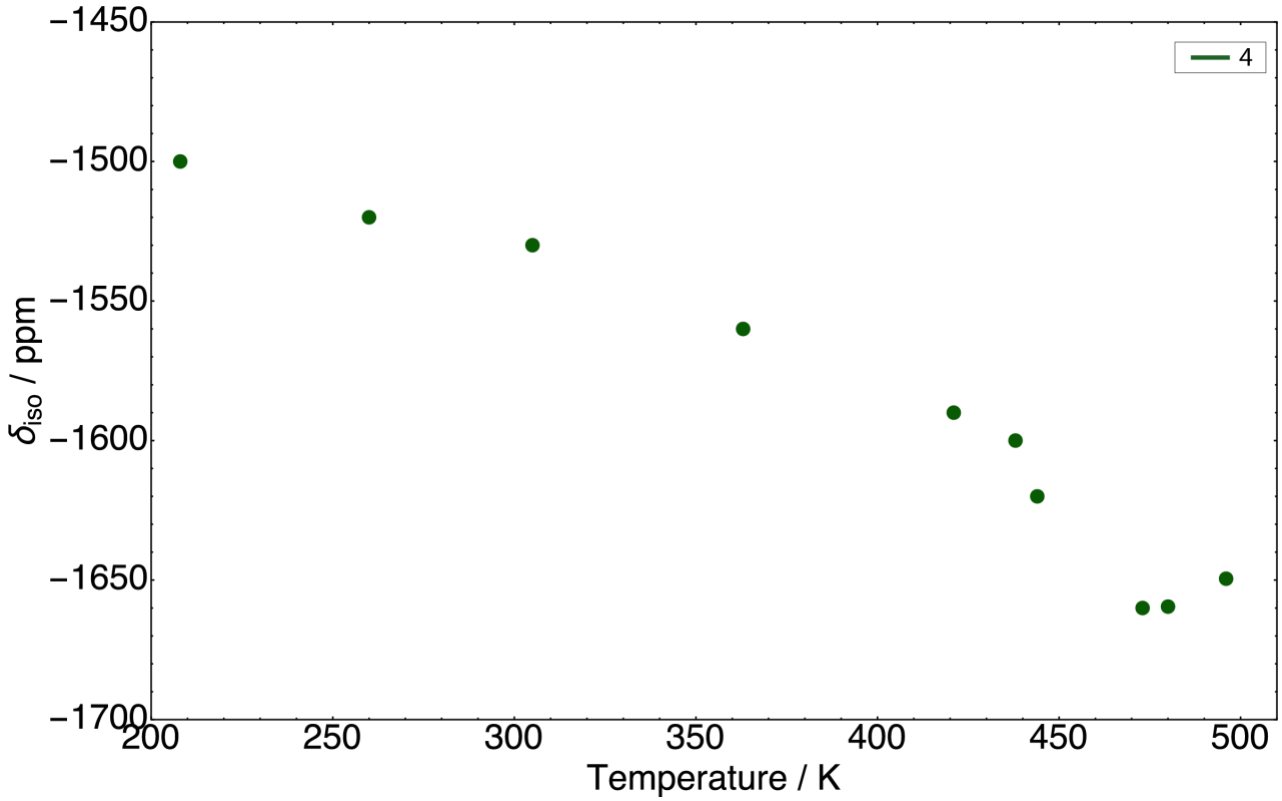

FIG. S8 continued. Temperature induced changes of ^{207}Pb chemical shift parameter δ_{iso} of site 4 in lead germanate.

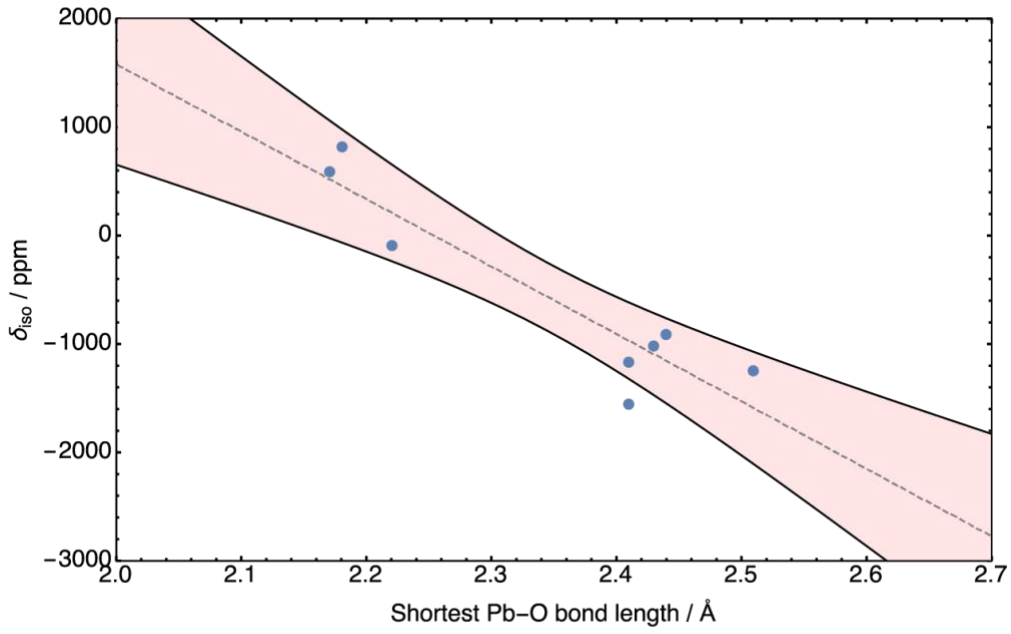

FIG. S9. Correlation between shortest Pb-O bond length and ^{207}Pb chemical shift parameter δ_{iso}, at 305 K. We do see a correlation, R = 0.90 for bond lengths from Kay et al. (blue points).

Table S2: Values of the shielding anisotropy (ζ) analyzed for each lead site at seven different temperatures. Sideband patterns were projected from TOP-aMAT spectra and individually fit using the method described in the main text. Entries formatted as X^{+Z}_{-Y} give the median ζ value for the $P(\zeta)$ distribution (neglecting infrequent outliers in the domain $\zeta < 0$) as X and the lower and upper 95% confidence limits as X-Y and X+Z, respectively. For site "5" at temperatures of 421 K and higher, the sign of ζ cannot be reliably discerned, and we report the properties of $P(|\zeta|)$. Here, the entries are formatted as 0^{+Z}, where $+Z$ is the one-sided 95% confidence limit.

Shielding Anisotropy, ζ / ppm										
Site	208 K	260 K	305 K	363 K	421 K	438 K	444 K	473 K	480 K	496 K
1B	2109^{+1103}_{-314}	2319^{+1156}_{-248}	2180^{+92}_{-89}	2211^{+91}_{-87}	1937^{+262}_{-465}	2017^{+327}_{-194}	*NA*	1973^{+134}_{-140}	2008^{+186}_{-160}	2129^{+83}_{-86}
1A	2121^{+174}_{-169}	2147^{+256}_{-173}	2116^{+56}_{-55}	2110^{+61}_{-61}	2006^{+107}_{-113}	2124^{+102}_{-92}	2162^{+135}_{-112}			
6	2296^{+133}_{-120}	2313^{+102}_{-102}	2325^{+96}_{-100}	2281^{+80}_{-195}	2215^{+113}_{-127}	2218^{+121}_{-112}	2180^{+117}_{-124}	2131^{+74}_{-72}	2018^{+99}_{-93}	2102^{+73}_{-69}
3B	1203^{+147}_{-133}	1244^{+93}_{-94}	1134^{+79}_{-77}	1060^{+66}_{-61}	977^{+73}_{-76}	909^{+83}_{-81}	1021^{+261}_{-201}			
5	1257^{+181}_{-163}	1345^{+145}_{-135}	1066^{+65}_{-63}	1117^{+56}_{-52}	1065^{+66}_{-62}	1063^{+66}_{-62}	1027^{+79}_{-74}	891^{+24}_{-25}	882^{+26}_{-27}	876^{+25}_{-26}
2A/2B	663^{+50}_{-47}	651^{+41}_{-37}	617^{+52}_{-53}	659^{+55}_{-57}	707^{+79}_{-79}	695^{+78}_{-74}	784^{+182}_{-142}	760^{+51}_{-49}	796^{+61}_{-58}	793^{+65}_{-60}
3A	647^{+40}_{-37}	676^{+35}_{-32}	656^{+41}_{-43}	659^{+44}_{-42}	688^{+36}_{-37}	664^{+46}_{-48}	631^{+58}_{-59}	697^{+69}_{-70}	720^{+80}_{-80}	788^{+81}_{-73}
4	356^{+122}_{-188}	423^{+71}_{-85}	263^{+41}_{-48}	229^{+48}_{-60}	0^{+170}	0^{+141}	0^{+210}	0^{+146}	0^{+129}	0^{+104}

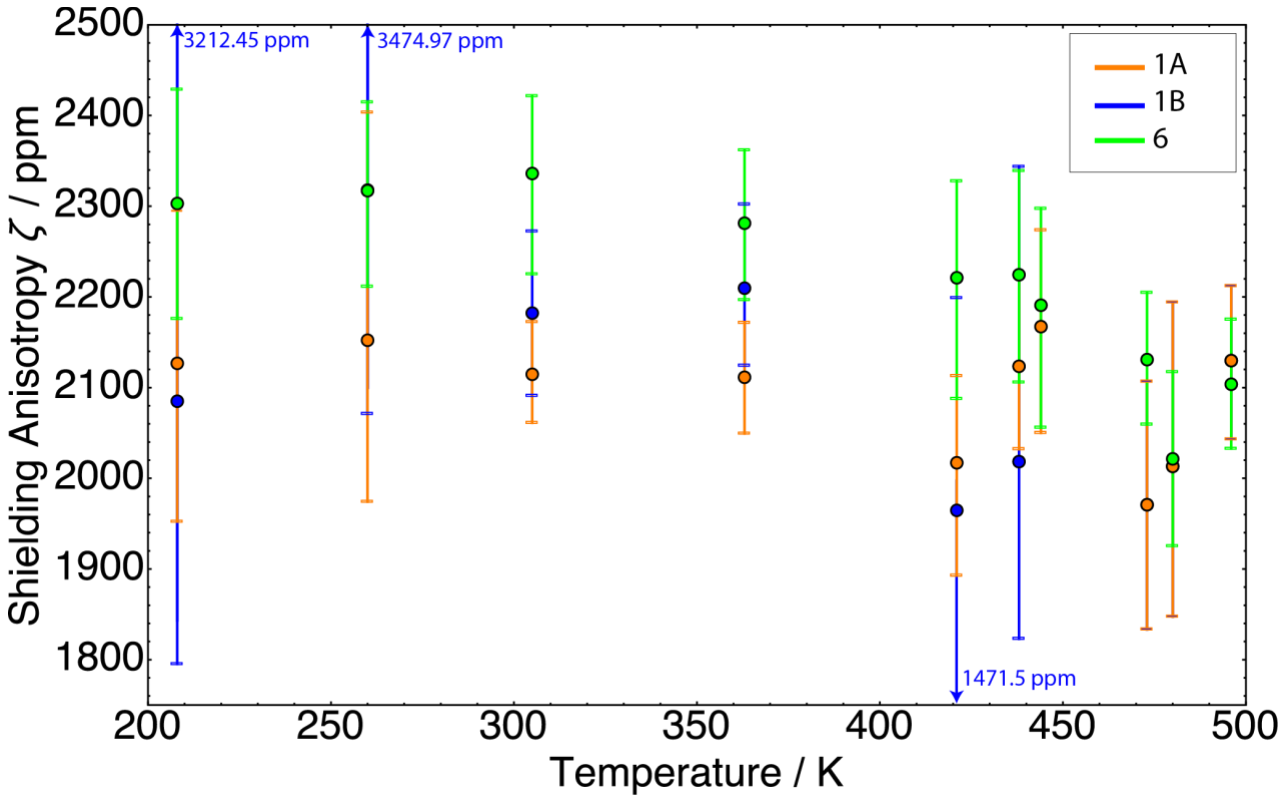

FIG. S10. Temperature induced changes of ^{207}Pb shielding anisotropy parameter ζ of downfield (deshielded) lead sites in lead germanate. Error bars on graph indicate the 95% confidence interval for the respective ζ parameter. $\Delta\zeta/\Delta T$ slopes are reported in Table S4. Points indicate best-fit for parameter.

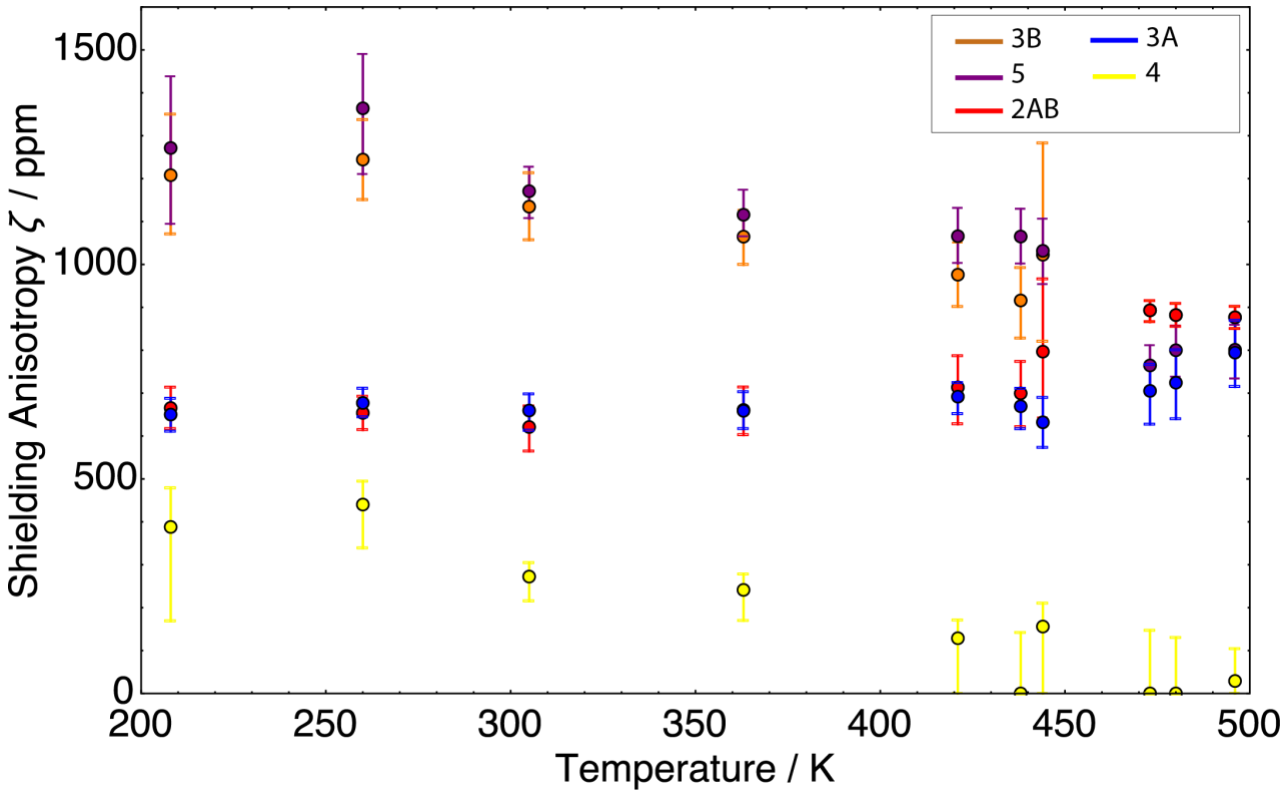

FIG. S11. Temperature induced changes of ^{207}Pb shielding anisotropy parameter ζ of upfield (shielded) lead sites in lead germanate. Error bars on graph indicate the 95% confidence interval for the respective ζ parameter. Δζ /ΔT slopes are reported in Table S4.

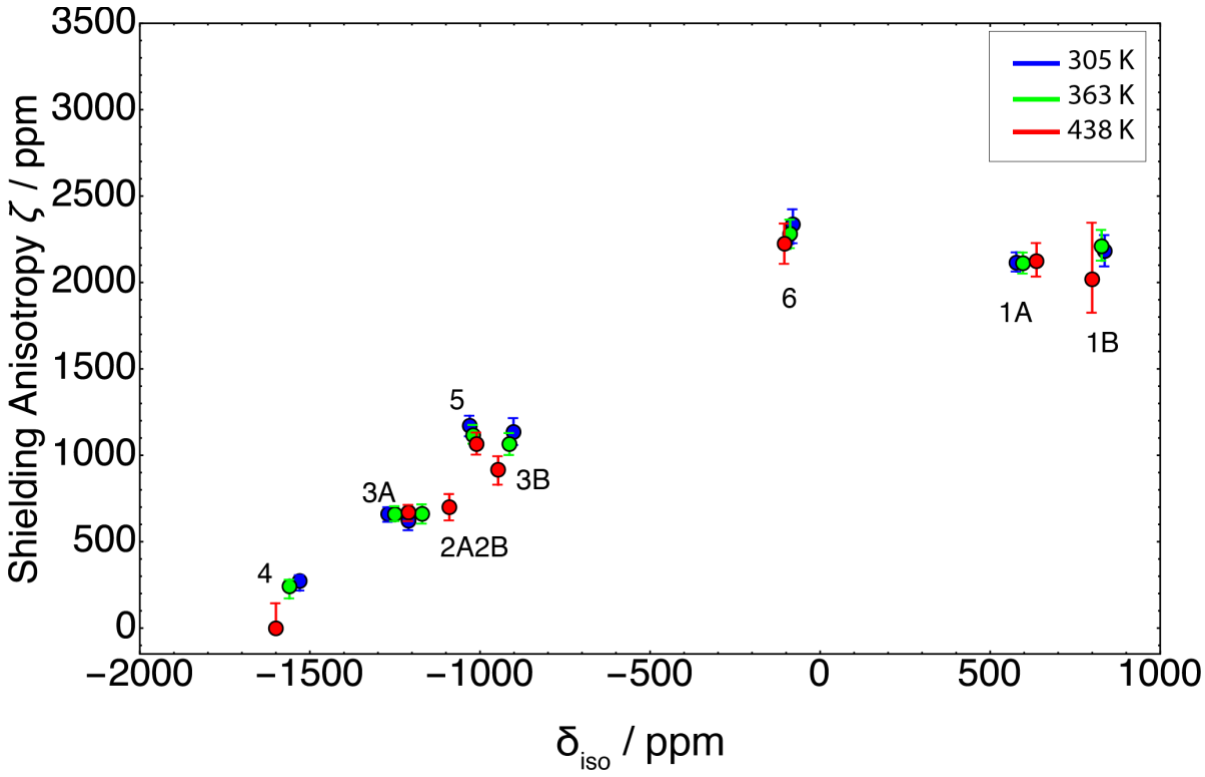

FIG. S12. Shielding anisotropy correlated to ^{207}Pb chemical shift in lead germanate at three different temperatures, 305 K (blue), 363 K (green), 438 K (red). Error bars indicate 95% confidence interval for shielding anisotropy parameter. Lead sites are labeled in black, temperatures are indicated on the graph.

Table S3: Values of the asymmetry parameter (η) analyzed for the given lead site at seven different temperatures. Sideband patterns were projected from TOP-aMAT spectra and individually fit using the method described in the main text. Entries formatted as X^{+Z}_{-Y} give the median ζ value for the $P(\eta)$ distribution as X and the lower and upper 95% confidence limits as X-Y and X+Z, respectively. For entries formatted as 0.00^{+Z}, $+Z$ is the one-sided 95% confidence limit. At each temperature, $P(\eta)$ for site 4 was approximately uniform across the entire domain over which η is defined (between zero and one), and hence is omitted from the table.

	Asymmetry parameter, η									
Site	208 K	260 K	305 K	363 K	421 K	438 K	444 K	473 K	481 K	496 K
1B	$0.00^{+0.53}$	$0.00^{+0.47}$	$0.16^{+0.09}_{-0.14}$	$0.16^{+0.09}_{-0.14}$	$0.00^{+0.35}$	$0.00^{+0.32}$	NA	$0.32^{+0.09}_{-0.09}$	$0.24^{+0.11}_{-0.15}$	$0.20^{+0.06}_{-0.09}$
1A	$0.25^{+0.16}_{-0.23}$	$0.27^{+0.14}_{-0.22}$	$0.20^{+0.05}_{-0.05}$	$0.23^{+0.04}_{-0.05}$	$0.00^{+0.15}$	$0.18^{+0.09}_{-0.15}$	$0.14^{+0.10}_{-0.12}$			
6	$0.00^{+0.22}$	$0.00^{+0.26}$	$0.00^{+0.15}$	$0.16^{+0.06}_{-0.10}$	$0.21^{+0.10}_{-0.14}$	$0.00^{+0.19}$	$0.11^{+0.10}_{-0.10}$	$0.17^{+0.07}_{-0.13}$	$0.00^{+0.18}$	$0.00^{+0.15}$
3B	$0.00^{+0.46}$	$0.00^{+0.44}$	$0.26^{+0.12}_{-0.22}$	$0.00^{+0.20}$	$0.31^{+0.15}_{-0.27}$	$0.00^{+0.29}$	$0.32^{+0.35}_{-0.30}$			
5	$0.00^{+0.44}$	$0.00^{+0.36}$	$0.00^{+0.17}$	$0.00^{+0.21}$	$0.00^{+0.25}$	$0.22^{+0.13}_{-0.20}$	$0.00^{+0.28}$	$0.00^{+0.27}$	$0.17^{+0.11}_{-0.15}$	$0.00^{+0.21}$
2A/2B	$0.00^{+0.42}$	$0.00^{+0.42}$	$0.00^{+0.37}$	$0.00^{+0.46}$	$0.00^{+0.52}$	$0.00^{+0.37}$	$0.00^{+0.46}$	$0.00^{+0.16}$	$0.00^{+0.29}$	$0.00^{+0.34}$
3A	$0.00^{+0.38}$	$0.00^{+0.40}$	$0.00^{+0.26}$	$0.37^{+0.17}_{-0.29}$	$0.00^{+0.31}$	$0.00^{+0.28}$	$0.27^{+0.27}_{-0.25}$	$0.00^{+0.27}$	$0.26^{+0.26}_{-0.24}$	$0.00^{+0.40}$

Table S4: Temperature dependence of ^{207}Pb site chemical shift parameters in $Pb_5(Ge_2O_7)(GeO_4)$ leading up to paraelectric phase transition (208 K to 438 K). At 473 K we observed a deviation from linear behavior. Data from Tables S1 and S2 was fit with a linear model, the standard error of each fit is reported. *The slope indicating the change in ζ with temperature for site 4 was only fit to 4 points, this is because above 363 K at an MAS of 12.5 kHz the CSA from this site was nearly completely removed and therefore an accurate sideband fit was not possible. The asymmetry parameter (η) did not change as a function of temperature (within the confidence band).

Site	$\Delta\delta_{iso}$ / ΔT (ppm / K)	Δζ / ΔT (ppm / K)
1B	-0.226 ± 0.024	-0.900 ± 0.455
1A	0.427 ± 0.024	-0.487 ± 0.211
6	-0.218 ± 0.017	-0.620 ± 0.170
3B	-0.390 ± 0.050	-1.374 ± 0.156
5	0.131 ± 0.0113	-1.683 ± 0.422
2A/2B	0.842 ± 0.034	0.630 ± 0.295
3A	0.484 ± 0.080	0.142 ± 0.063
4*	-0.436 ± 0.026	-1.172 ± 0.578

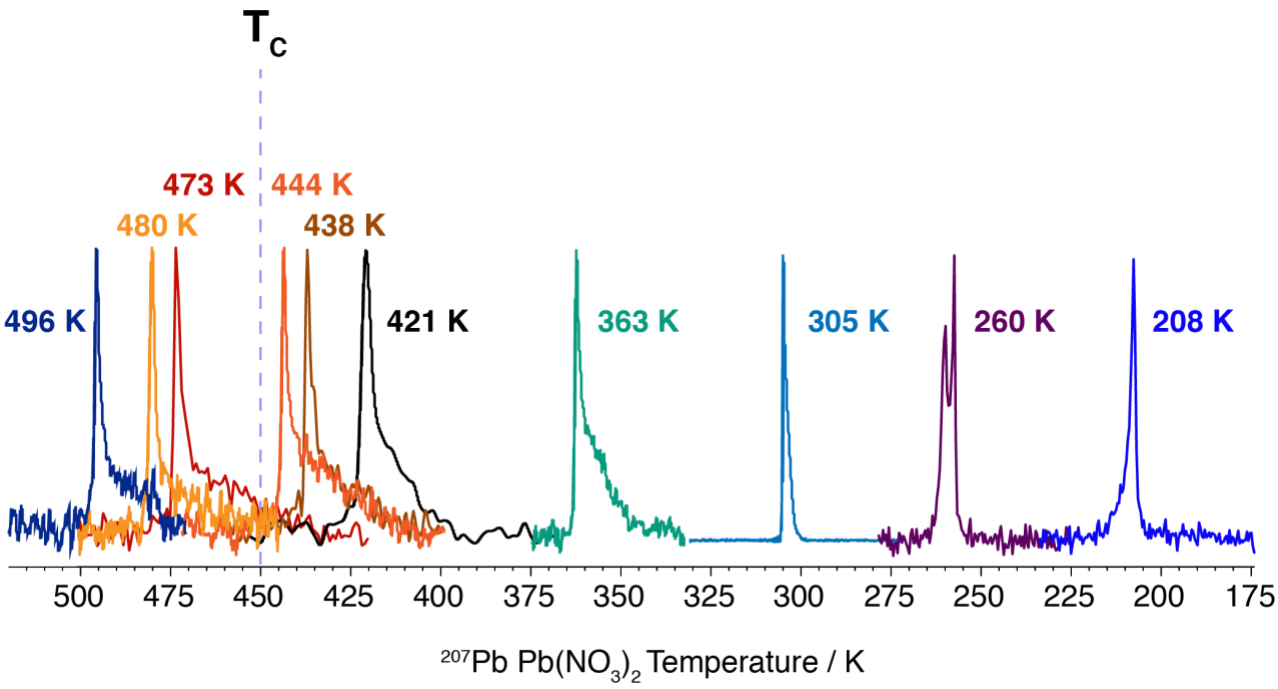

FIG. S13. Using the $Pb(NO_3)_2$ ^{207}Pb chemical shift as a thermometer[12]: we measure the temperature gradient across an MAS rotor at temperature settings used for TOP-aMAT lead germanate experiments. 12.5 kHz (>305 K), 20 kHz (208 K and 260 K). The temperatures indicated on the left hand side of each figure indicates the temperature calculated from the ^{207}Pb chemical shift with the maximum intensity. The dotted line indicates the Curie temperature of lead germanate.

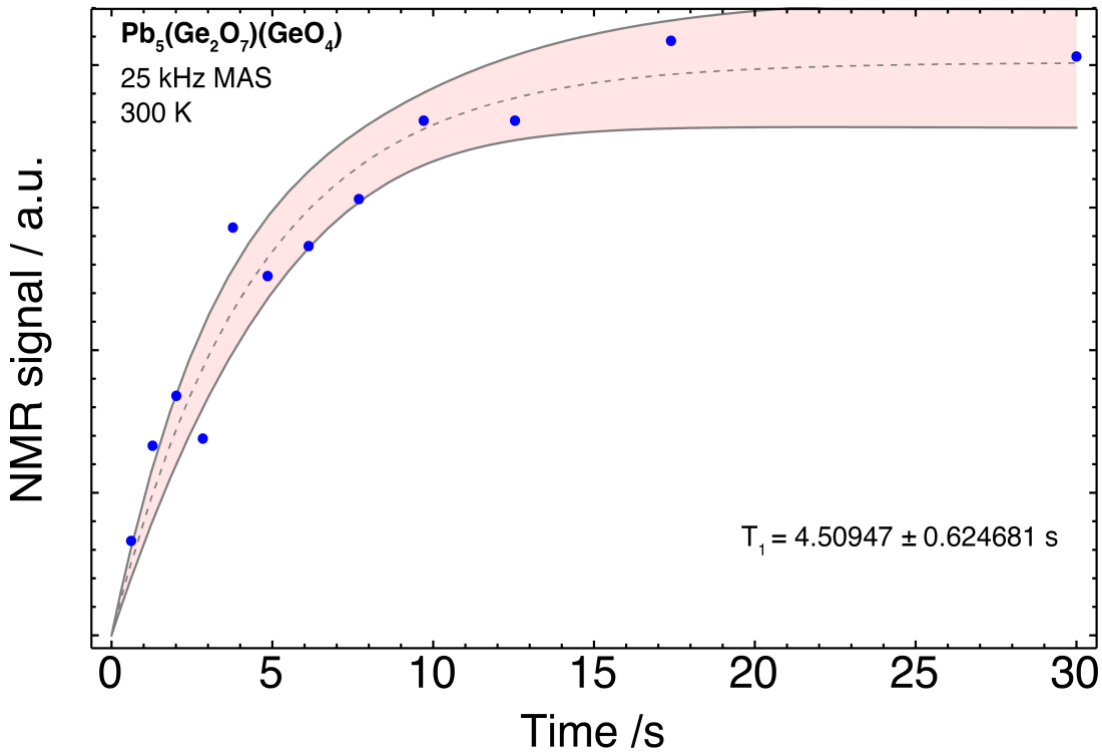

FIG. S14. Spin-lattice relaxation of lead germanate (integration done across all lead sites). Taken at 300 K with an MAS rate of 25 kHz. Points were fit to a single exponential, giving a T1 time of 4.5 seconds at room temperature.

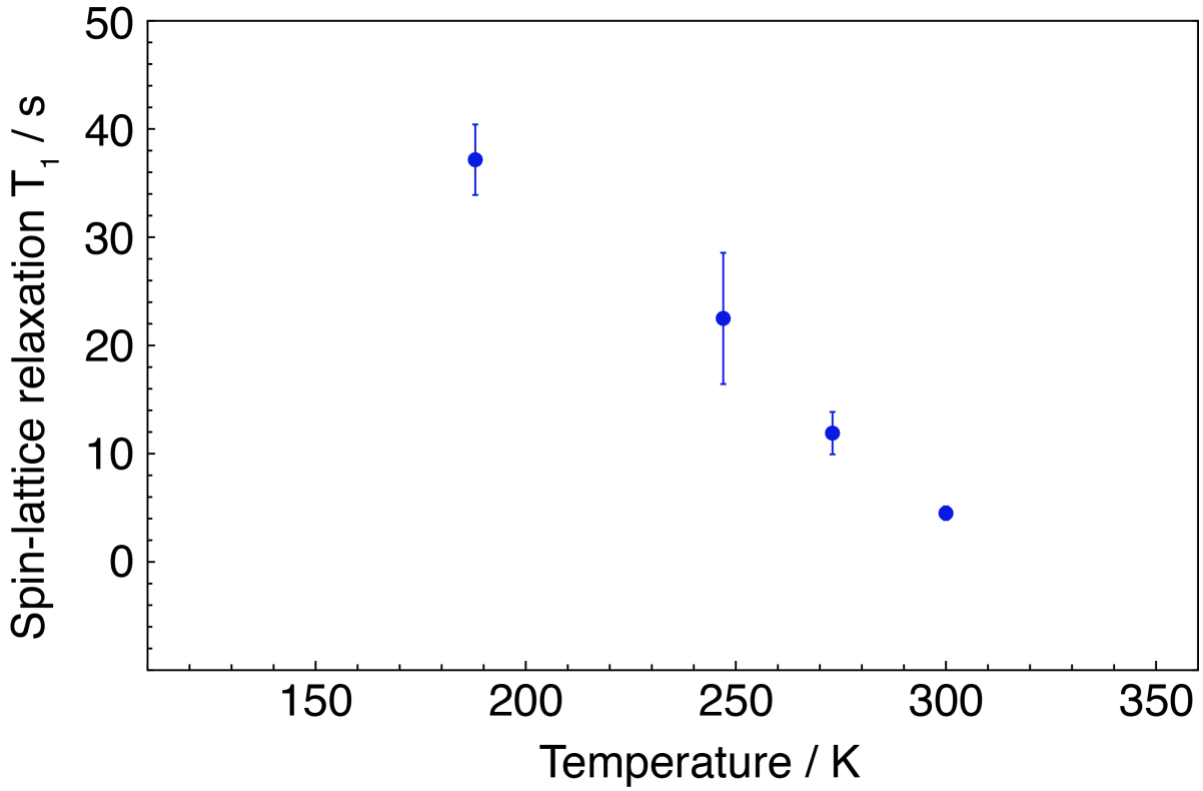

FIG. S15. Spin-lattice relaxation of ^{207}Pb lead sites in lead germanate (integration done across all lead sites). Taken at variable temperature with an MAS rate of 12.5 kHz. Points were fit to a single exponential.

Table S5: Experimental parameters used for TOP-aMAT experiments. The echo shift was 1 rotor period between the fifth and sixth tanh/tan pulses. This allowed for sufficient early acquisition to reconstruct a full half-echo without any phasing artifacts using TOP. Other spectral artifacts related to short transverse relaxation times could persist but would be difficult to distinguish given the signal-to-noise ratios of our experiments.

Parameter list for each TOP-aMAT experiments										
Parameters	208 K	260 K	305 K	363 K	421 K	438 K	444 K	473 K	480 K	496 K
Rabi ν_1(^{207}Pb) / kHz	312	312	303	303	303	312	250	250	250	250
SHAP width (MHz)	8	8	8	8	8	8	8	8	8	8
MAS (kHz)	20	20	12.5	12.5	12.5	12.5	12.5	12.5	12.5	12.5
Transmitter offset (ppm)	661.534	661.534	661.534	661.534	1019.916	661.534	661.534	661.534	554.711	554.711
Recycle delay (s)	14	9	6.125	4.5	3.5	3.5	3	3	3	3
Number of Points	8192	8192	4096	8192	8192	8192	8192	8192	8192	8192
Experiment time (hours)	17.51	18.78	47.45	36.09	88.02	89.89	89.89	89.89	67.3	86.9
Number of scans	180	300	696	720	2256	2304	2880	2880	2016	2604

V. EXCHANGE MODEL

We use modified Bloch equations, the McConnell equations[13], to describe interconversion between the L and D enantiomorphic forms of lead germanate. We do a simultaneous fit of seven sets of spectral data taken at temperatures above 400 K. We use the following form of the McConnell equation: (S1):

$$S[v] = Re[\frac{2(2Ae^{-\frac{E_a}{R_m T}} + R + i\pi(2v - b_A + m_A T) - (b_X + m_X T))}{(R + 2i\pi(v - (b_A + m_A T)))(R + 2i\pi(v - (b_X + m_X T)) + 2Ae^{-\frac{E_a}{R_m T}}(R + i\pi(2v - (b_A + m_A T) - (b_X + m_X T))}]$$

Where E_a is the activation energy, R_m is the gas constant, T is the temperature, A is the pre-exponential factor of the Arrhenius equation, v is the spectral frequency, $b_A + m_A T$ is the temperature dependent frequency offset for site A (ν_A) and $b_X + m_X T$ is the temperature dependent frequency offset for site X (ν_B). The R parameter takes into account the intrinsic linewidth of the nuclear spin resonances in the absence of exchange as well as any broadening effects on the lineshape due to temperature gradients. The fit was performed using Wolfram Mathematica 11.3.0.0.0, parameters and confidence intervals at 95% were obtained using the Nonlinearmodelfit function.

Table S6: Temperature dependent frequency offsets for sites 1A and 1B obtained from simultaneous fit of 421 K, 438 K, 444 K, 473 K, 480 K and 496 K TOP-aMAT isotropic chemical shift projections.

	421 K	438 K	444 K	473 K	480 K	496 K
$\nu_A(^{207}Pb)$ / ppm	807	803	801	793	791	786
$\nu_B(^{207}Pb)$ / ppm	636	638	640	650	652	657

REFERENCES

1. Kay, M. I.; Newnham, R. E.; Wolfe, R. W., Crystal-Structure of Ferroelectric Phase of Pb5ge3o11. *Ferroelectrics* **1975,** *9* (1-2), 1-6.
2. Te Velde, G.; Bickelhaupt, F. M.; Baerends, E. J.; Guerra, C. F.; Van Gisbergen, S. J. A.; Snijders, J. G.; Ziegler, T., Chemistry with ADF. *J Comput Chem* **2001,** *22* (9), 931-967.
3. Guerra, C. F.; Snijders, J. G.; te Velde, G.; Baerends, E. J., Towards an order-N DFT method. *Theor Chem Acc* **1998,** *99* (6), 391-403.
4. Baerends, E. J. a. Z., Tom and Atkins, A. J. and Autschbach, Jochen and Bashford, Donald and Baseggio, O. and Bérces, A. and Bickelhaupt, F. Matthias and Bo, C. and Boerritger, P. M. and Cavallo, Luigi and Daul, C. and Chong, D. P. and Chulhai, D. V. and Deng, L. and Dickson, R. M. and Dieterich, J. M. and Ellis, D. E. and van Faassen, M. and Ghysels, A. and Giammona, A. and van Gisbergen, Stan J. A. and Goez, A. and Götz, A. W. and Gusarov, S. and Harris, F. E. and van den Hoek, P. and Hu, Z. and Jacob, Christoph R. and Jacobsen, H. and Jensen, L. and Joubert, L. and Kaminski, J. W. and van Kessel, G. and König, C. and Kootstra, F. and Kovalenko, A. and Krykunov, Mykhaylo and van Lenthe, Erik and McCormack, D. A. and Michalak, A. and Mitoraj, M. and Morton, S. M. and Neugebauer, Johannes and Nicu, V. P. and Noodleman, Louis and Osinga, V. P. and Patchkovskii, S. and Pavanello, Michele and Peeples, C. A. and Philipsen, Pierre Herman Theodoor and Post, D. and Pye, Cory C. and Ramanantoanina, H. and Ramos, P. and Ravenek, W. and Rodríguez, J. I. and Ros, P. and Rüger, R. and Schipper, P. R. T. and Schüns, D. and van Schoot, H. and Schreckenbach, G. and Seldenthuis, J. S. and Seth, Mike and Snijders, Jaap G. and Solà, Miquel and Stener M. and Swart, M. and Swerhone, D. and te Velde, G. and Tognetti, V. and Vernooijs, P. and Versluis, L. and Visscher, Lucas and Visser, O. and Wang, Fan and Wesolowski, T. A. and van Wezenbeek, E. M. and Wiesenekker, G. and Wolff, S. K. and Woo, T. K. and Yakovlev, A. L. *ADF2017, SCM, Theoretical Chemistry, Vrije Universiteit, Amsterdam, The Netherlands,* https://www.scm.com/ *(misc)*, 2017.

5. vanLenthe, E.; vanLeeuwen, R.; Baerends, E. J.; Snijders, J. G., Relativistic regular two-component Hamiltonians. *Int J Quantum Chem* **1996,** *57* (3), 281-293.
6. Autschbach, J., Perspective: Relativistic effects. *J Chem Phys* **2012,** *136* (15).
7. van Lenthe, E.; Ehlers, A.; Baerends, E. J., Geometry optimizations in the zero order regular approximation for relativistic effects. *J Chem Phys* **1999,** *110* (18), 8943-8953.
8. Vanlenthe, E.; Baerends, E. J.; Snijders, J. G., Relativistic Total-Energy Using Regular Approximations. *J Chem Phys* **1994,** *101* (11), 9783-9792.
9. Grimme, S.; Antony, J.; Ehrlich, S.; Krieg, H., A consistent and accurate ab initio parametrization of density functional dispersion correction (DFT-D) for the 94 elements H-Pu. *J Chem Phys* **2010,** *132* (15).
10. Alkan, F.; Dybowski, C., Calculation of chemical-shift tensors of heavy nuclei: a DFT/ZORA investigation of Hg-199 chemical-shift tensors in solids, and the effects of cluster size and electronic-state approximations. *Phys Chem Chem Phys* **2014,** *16* (27), 14298-14308.
11. Alkan, F.; Dybowski, C., Chemical-shift tensors of heavy nuclei in network solids: a DFT/ZORA investigation of Pb-207 chemical-shift tensors using the bond-valence method. *Phys Chem Chem Phys* **2015,** *17* (38), 25014-25026.
12. Kemp, T. F.; Balakrishnan, G.; Pike, K. J.; Smith, M. E.; Dupree, R., Thermometers for low temperature Magic Angle Spinning NMR. *J Magn Reson* **2010,** *204* (1), 169-172.
13. Mcconnell, H. M., Reaction Rates by Nuclear Magnetic Resonance. *J Chem Phys* **1958,** *28* (3), 430-431.